LEVEL II

Final Report

CONTINUATION OF SPACE-ARRAY PROGRAM

By: M. S. FRANKEL R. A. LONG R. A. NELSON W. A. EDSON

Prepared for:

DEFENSE COMMUNICATIONS AGENCY
WASHINGTON, D.C. 20305

CONTRACT DCA100-77-C-0031

Sponsored by

DEFENSE ADVANCED RESEARCH PROJECTS AGENCY
ARPA ORDER 2645

SRI

STANFORD RESEARCH INSTITUTE
Menlo Park, California 94025 · U.S.A.

STANFORD RESEARCH INSTITUTE
Menlo Park, California 94025 · U.S.A.

Final Report *October 1977*

CONTINUATION OF SPACE-ARRAY PROGRAM

By: M. S. FRANKEL R. A. LONG R. A. NELSON W. A. EDSON

Prepared for:

DEFENSE COMMUNICATIONS AGENCY
WASHINGTON, D.C. 20305

CONTRACT DCA100-77-C-0031

ARPA ORDER 2645

SRI Project 6247

Approved by:

DAVID A. JOHNSON, *Director*
Radio Physics Laboratory

RAY L. LEADABRAND, *Executive Director*
Electronics and Radio Sciences Division

Copy No. 5

SECURITY CLASSIFICATION OF THIS PAGE (When Data Entered)

REPORT DOCUMENTATION PAGE

READ INSTRUCTIONS BEFORE COMPLETING FORM

1. REPORT NUMBER

2. GOVT ACCESSION NO.

3. RECIPIENT'S CATALOG NUMBER

4. TITLE (and Subtitle)

(10) CONTINUATION OF SPACE-ARRAY PROGRAM

5. TYPE OF REPORT & PERIOD COVERED
Final Report
Covering the period 21 March to 21 September 1977

6. PERFORMING ORG. REPORT NUMBER
SRI International Project 6247

7. AUTHOR(s)

(10) Michael S. Frankel, Roy A. Long
Ray A. Nelson, William A. Edson

8. CONTRACT OR GRANT NUMBER(s)
Contract DCA100-77-C-0031

9. PERFORMING ORGANIZATION NAME AND ADDRESS
SRI International
Menlo Park, California 94025

10. PROGRAM ELEMENT, PROJECT, TASK AREA & WORK UNIT NUMBERS
ARPA Order 2645

11. CONTROLLING OFFICE NAME AND ADDRESS
Defense Communications Agency
Washington, D.C. 20305

(11) 12. REPORT DATE
20 October 1977

13. NO. OF PAGES
76

15. SECURITY CLASS. (of this report)
Unclassified

14. MONITORING AGENCY NAME & ADDRESS (if diff. from Controlling Office)

(15) DCA100-77-C-0031,
VV ARPA Order-2645

15a. DECLASSIFICATION/DOWNGRADING SCHEDULE

16. DISTRIBUTION STATEMENT (of this report)

Approved for public release;
distribution unlimited.

17. DISTRIBUTION STATEMENT (of the abstract entered in Block 20, if different from report)

(9) Final rept. 21 Mar-21 Sep 77,

18. SUPPLEMENTARY NOTES

(12) 69 p. (18) SBIE (19) AD-E100 443

19. KEY WORDS (Continue on reverse side if necessary and identify by block number)

Passive satellite
PACSAT
Libration damping
Flexure damping
Limited-motion joints
Libration-damping springs

20. ABSTRACT (Continue on reverse side if necessary and identify by block number)

Experiments were conducted to evaluate the coefficient of friction, μ_s, in the PACSAT limited-motion joints and the resulting libration damping characteristics of the springs attached to the ends of the array. Measurements for μ_s between surfaces burnished with pure molybdenum disulfide (a solid-film lubricant) show that this coefficient can be made independent of tension in the joints. Measurements made in a vacuum for the lubricated surfaces gave $\mu_s = 0.4$. This value for the coefficient of friction in the PACSAT joints would result in no measurable degradation ($\lesssim 0.1$ dB) in the array's radar cross section as a

(cont.)

DD FORM 1 JAN 73 1473
EDITION OF 1 NOV 65 IS OBSOLETE

SECURITY CLASSIFICATION OF THIS PAGE (When Data Entered)

410 281

19. KEY WORDS (Continued)

20 ABSTRACT (Continued)

consequence of friction in the joints; and in a geostationary array this friction gives rise to a damping of tip displacement, due to flexure, of about 2 cm per day. This damping of the primary flexural mode of oscillation for the array is adequate for future PACSAT applications.

The experiments to measure the libration-damping characteristics of the springs to be attached to the ends of the array did not provide conclusive results. This situation arose because a very large torsional pendulum was required to measure the damping coefficient of these springs when subjected to torsional strains with six-hour periods (as they would be for a PACSAT in a synchronous orbit). The size of this pendulum resulted in its being very sensitive to spurious perturbations. Although no quantitative data were obtained from this experiment, it was observed that springs made from cadmium plated beryllium copper wire tend to damp torsional flexures with six-hour periods more than do springs made of unplated wire. More definitive torsional pendulum experiments could be performed in a vacuum chamber, but they would require a large and costly facility.

6-hour

iv

CONTENTS

ILLUSTRATIONS

TABLES

I INTRODUCTION

The usefulness of satellites for both communication and navigation is now established beyond doubt. A great variety of satellites are in current use, and additional satellites for a variety of purposes are being prepared and launched. All of the satellites presently in use are active in the sense that they either amplify signals delivered to them from an earth station or independently generate signal power.

Passive satellites that provide a communication channel by reflecting earth-originated signals have been investigated in the past--for example, through the Echo and West Ford experiments. However, no operational system has resulted from this work. The present PACSAT (Passive Communication Satellite) project is concerned with a new form of satellite that shows promise for meeting certain special communication requirements. Figure 1 is an artist's conception of a transatlantic communication link using a satellite of this kind in synchronous orbit.* Signals transmitted toward the satellite from Europe are returned to a receiving station in the United States.

This satellite differs from previous passive satellites in that it consists of a large number of scattering elements, arranged in an orderly array so that coherent addition of scattered energy forms the return signal. The principles that govern the array operation are presented in Figure 2. The signal returned to earth is concentrated in a thin-walled hollow cone that intersects the earth in a circular pattern centered on the subsatellite point. Varying the wavelength of the signal changes the radius of this circle. Only one lobe is returned to earth if the spacing, s, between array elements lies in the range between $\lambda/2$ and λ.

---

*The PACSAT can be used in lower-altitude orbits. The choice of synchronous orbit in the figure is intended only as an example.

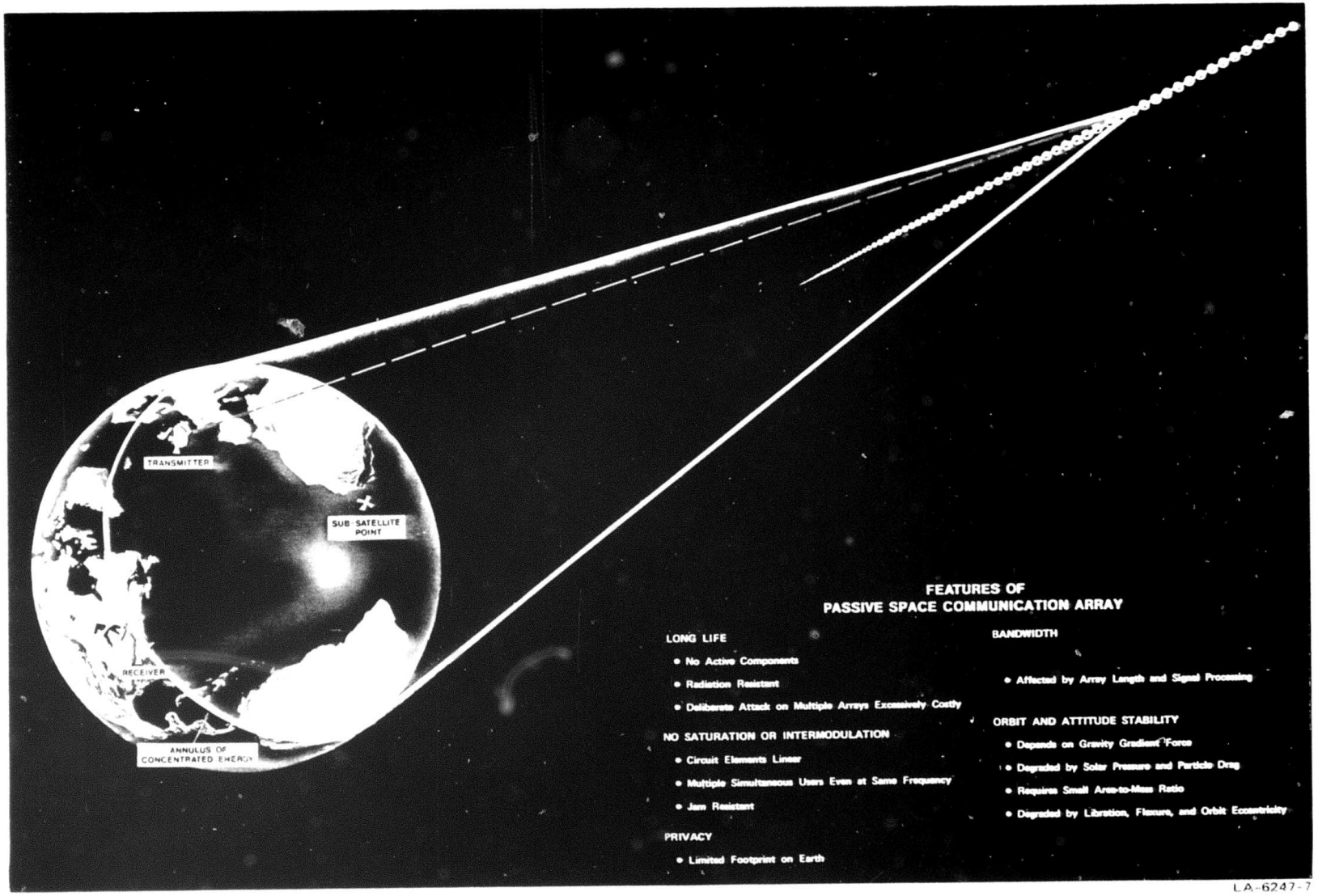

FIGURE 1 FEATURES OF PASSIVE SPACE COMMUNICATION ARRAY

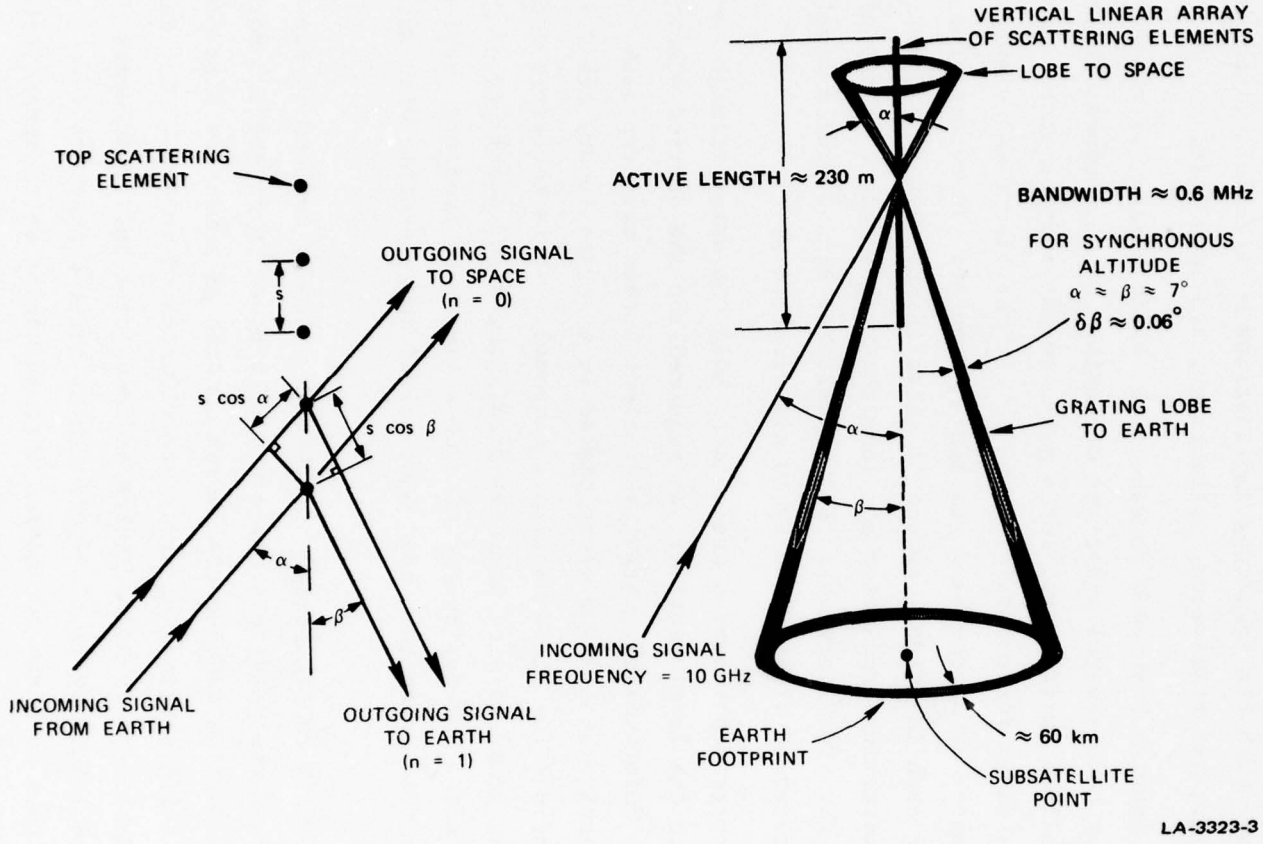

FIGURE 2 RESPONSE OF A COLUMNAR ARRAY OF ISOTROPIC SCATTERERS

It is emphasized that the coverage and orbital properties of this satellite are essentially the same as those of any other synchronous satellite. The principal difference is the absence of active elements in the array, with the resulting implications of simplicity, economy, survivability, jam resistance, reliability, and long life.

Metal spheres have been chosen as the basic element of the array because they meet several important criteria. Of all shapes, the sphere has the smallest surface area for a given volume and therefore mass. This is desirable for orbital reasons. From the electrical viewpoint, a resonant sphere is a broadband scattering element. Therefore, the behavior of each individual sphere is quite insensitive to frequency. Also the scattering properties are completely independent of the direction from which the signal arrives, so the scattered signal from a single sphere is returned almost equally in all directions.

Gravity-gradient forces are used to hold the array straight and aligned with the local vertical, as required for the desired electrical operation. Unfortunately, gravity-gradient forces are very weak. The greatest tension in a 230-m array placed in a geostationary orbit is of the order of 6×10^{-5} newtons (i.e., 6 dynes). It is therefore necessary to take great care to preserve straightness and stability of attitude. Also, the deployment of such a structure presents problems that differ from those that have been solved in connection with existing satellites.

The overall configuration of a PACSAT intended to demonstrate the feasibility of the passive array concept is shown in Figure 3. Both the central portion and the tip masses consist of nominally straight, relatively stiff sections of array, as illustrated in Figure 4. Each section consists of 99 normal balls and one joint ball. Adjacent sections are joined by limited-motion ball-joint connectors (see Figure 5), that are free for motion through angles up to approximately 3°. Both of the bearing surfaces in each joint are coated with molybdenum disulfide, a space-qualified solid lubricant.

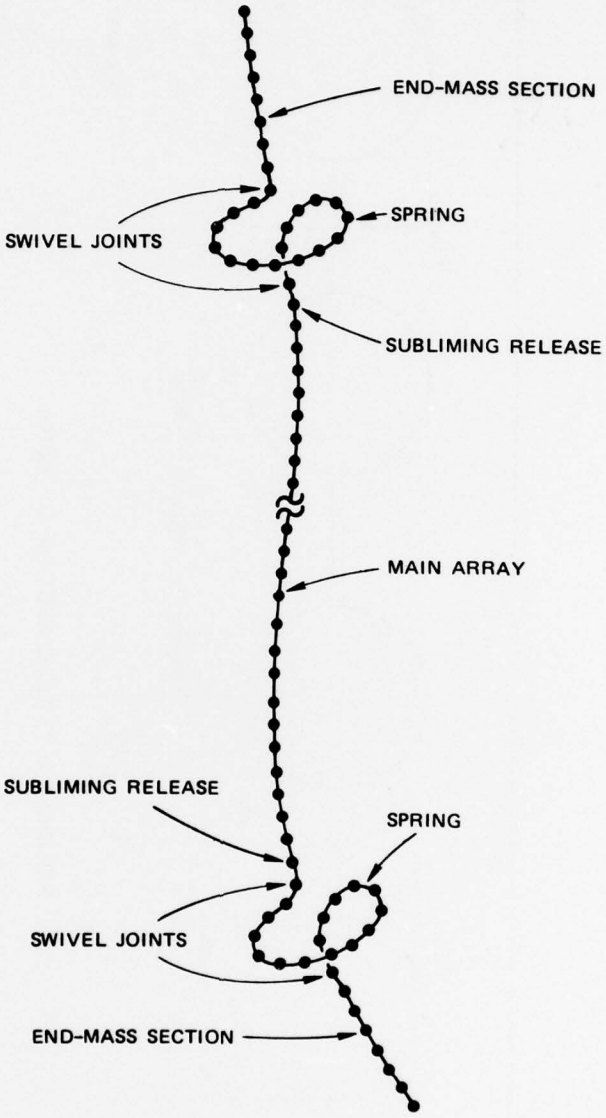

FIGURE 3 PACSAT CONFIGURATION

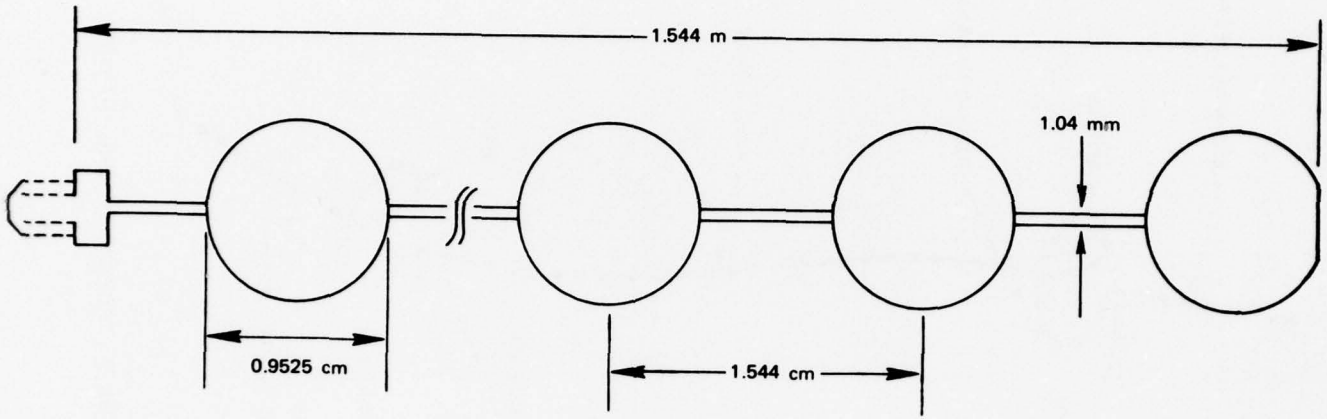

FIGURE 4 TYPICAL SECTION OF ARRAY

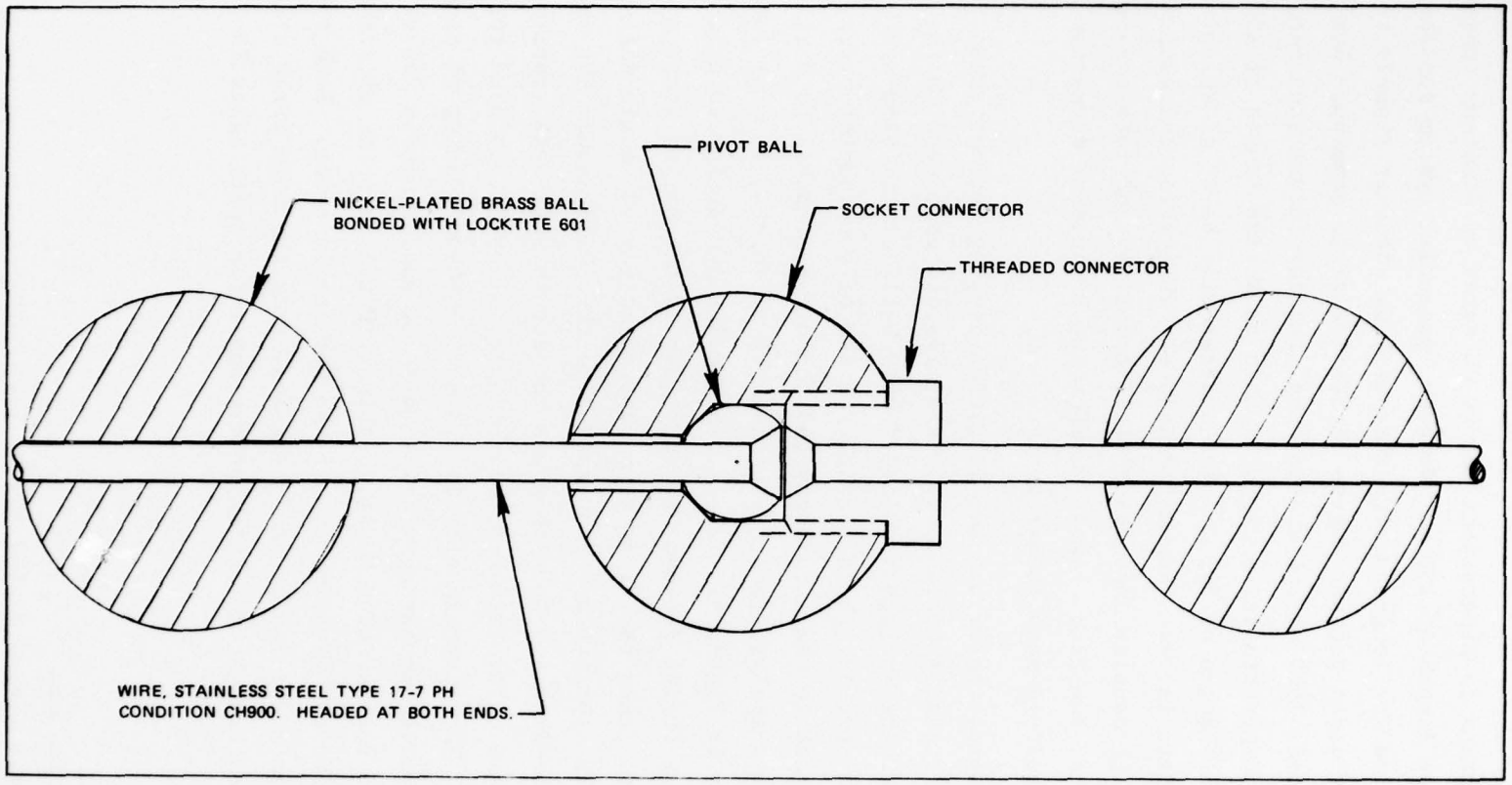

FIGURE 5 LIMITED-MOTION BALL JOINT

Early design considerations led to an array of aluminum spheres with an active length of 150 m. However, potential system applications indicate a need for longer arrays that provide stronger signals to the intended user and a greater degree of resistance to jamming. Arrays of aluminum spheres 1500 m long are contemplated for future launches; however, the demonstration array will have an active length of 230 m and an overall length of 300 m. The spheres will be of nickel-plated brass; this material was chosen for ease of fabrication and because its relatively high density improves orbital stability and increases the confidence that the same stowage chamber and deployment mechanism can be used to deploy a much longer array.

The construction of the two libration-damping springs shown in Figure 3 (for details see Ref. 1)* is similar to that used in the main array, in that the springs are loaded with balls of the same size, material, and spacing. Each spring consists of one complete turn, with one end attached to the main array and the other attached to a tip mass. The attachments are provided by special swivel joints, as indicated schematically in Figure 6. These joints allow the spring to be in line with the array during deployment; subsequently the spring forms a one-turn coil that joins the array at an approximately 90° angle during operation. The springs are prestressed so they will assume the desired shape after deployment, when they are subject to very weak gravity-gradient forces. Tempered beryllium copper, alloy 25, is used for the spring wire. The wire diameter is 0.3 mm. A 50-μm plating of cadmium over the beryllium copper provides damping of approximately 20% of the energy in the spring, each cycle; a thin (≈10 μm) flashing of silver over the cadmium prevents sublimation of the cadmium in space. Both springs and tip masses are released and drift away from the main array after four to six months through the action of the subliming split balls (see Figure 3).

*References are listed at the end of this report.

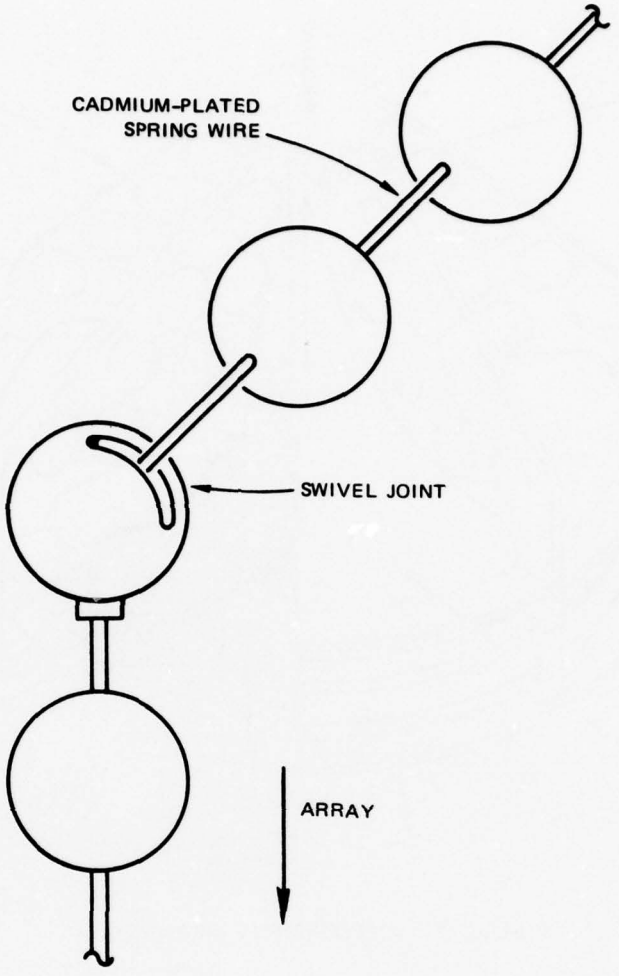

FIGURE 6 DAMPING-SPRING JOINTS

The deployment mechanism* for the PACSAT is shown in Figure 7. The array is stored in a circular canister or chain locker and is suitably constrained so that the vibrations encountered during the launch will not injure the array or its associated mechanisms. Between launch and deployment the constraint is released and the array is tranquil within the container. When the launch command is received, a pair of belts gripping

*This mechanism was designed to allow the array to ride piggyback with a pair of 777 satellites that are launched with a Titan III-C rocket.

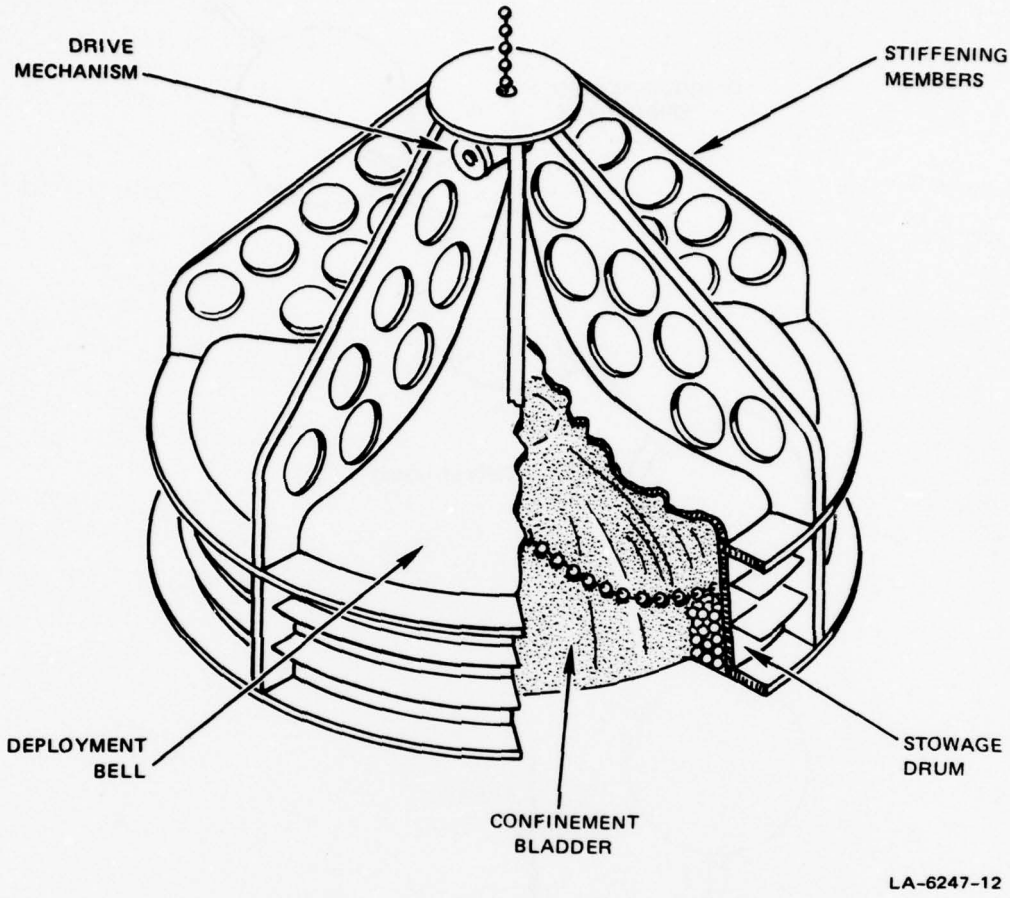

FIGURE 7 DEPLOYMENT MECHANISM

the array is accelerated to a surface speed of one meter per second and the array is ejected toward the nadir. The deployment process ends when the array leaves the drive belt.

In the foregoing discussion it is implicitly assumed that (1) the coefficient of static friction, μ_s, in the limited-motion joints is sufficiently low that the array will hang straight where subjected to the very small gravity-gradient forces; (2) friction in the joints provides adequate damping of flexure motions in the array; and (3) the libration-damping springs will dissipate energy when subjected to torsional flexures

with 6-hour periods.* This report presents the results of experiments that were implemented in an attempt to verify these assumptions.

In addition to reporting these results, this report describes several examples of communication links using the PACSAT, and it presents an analysis on the straightness required of the array when used in the link. This requirement will also be addressed in light of the experimental values obtained for the friction coefficient in the limited-motion joints.

*This period is appropriate for a PACSAT in a geostationary orbit.

II PACSAT COMMUNICATION LINKS

A. General

To form a basis for estimating possible future uses for passive satellites, we have investigated the feasibility of implementing an aircraft-to-aircraft communication link via PACSAT. Interest in this link arises because of the possibility of using the array for communication between the National Command Authority aircraft and the Armed Forces. The subsections that follow show how such a link might be designed.

B. An Aircraft-to-Aircraft PACSAT Link

We assume that a broadcast* link between designated aircraft is to be established at a nominal frequency of 8 GHz. Because PACSAT does not provide "gain" (as does an active satellite), relatively large apertures are required for the transmitter and receiver antennas to broadcast a given message in a ~10-minute interval† to all possible receivers within a predefined region.

A survey of present technology indicates that adequate antenna apertures can be obtained by using conformal phased arrays. Mr. Robert Munsen at Ball Brothers has informed us that X-band arrays of these types can be built with the following characteristics:

- Main beam steerable over at least ±45° from normal to array
- Input power handling capability ~1 kW (CW)
- Array "thickness" on the order of 1.27 cm (0.5 inch)
- Array widths and lengths up to at least 10 m
- Array efficiency greater than 50%.

---

*In this report we define a broadcast link as one that provides complete coverage over a prespecified segment of the earth's surface.

†This time requirement arises from a particular application identified for the PACSAT.

These arrays are very attractive for the PACSAT application, and one might assume that it is necessary only to select a sufficiently large array to satisfy the link requirements. However, our analysis shows that the cost-effectiveness of a PACSAT system can be increased by making a tradeoff between the number of PACSATs* in orbit and the size of the transmitting and receiving apertures. This tradeoff must be made because the cost of making and launching passive satellites is expected to be significantly less than that required to place "large" (e.g., 3 m by 9 m) conformal arrays on an extensive fleet of aircraft. A preliminary cost analysis has been made, and the link discussed in the next subsection is felt to represent a near-optimum compromise in the tradeoff that exists between these parameters.

1. Link Margin Calculations

We envisage a system in which several PACSATs are placed in a circular polar orbit at an altitude of 10,000 km (~5400 nmi), which results in an orbital period of ~5.5 hours. This geometry is shown, to scale, in Figure 8.

Simple calculations show that if coverage is to be provided for all points above 30°N latitude,† then one PACSAT per 14° of the orbit is required. Hence, the total number of satellites is (360°/14°) = 26, a number that we double to 52 to ensure (with high probability) that an array is always available for establishing the link. These numbers are based on the assumption that service may extend to zero-degree elevation angles, which is believed to be reasonable because the terminals will be airborne, resulting in little atmospheric attenuation of the transmitted and received signals for these takeoff angles.

---

*The number of PACSATs in any predescribed orbit is governed by a requirement to provide continuous coverage to all stations within the broadcast region. As the orbital altitude becomes lower, the number of required satellites increases; however, spreading losses for the signals decrease and the required aperture sizes decrease.

†This zone of coverage is representative of a potential application identified for the PACSAT.

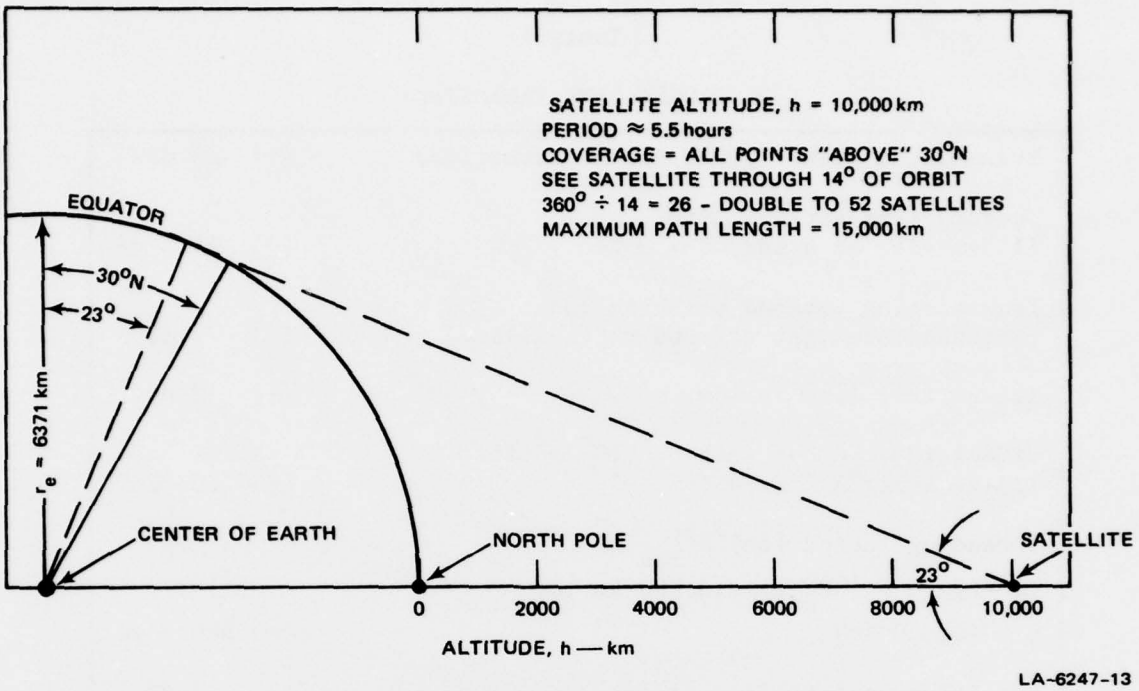

FIGURE 8 ORBITAL GEOMETRY

Figure 8 also shows that: (1) the worst-case, one-way signal path length is ~15,000 km, and (2) the half-cone angle of the coverage zone for each satellite is ~23°. Based on these numbers, and the assumption that a maximum desirable receiving array size is 3 m by 3 m,* we have the system parameters listed in Table 1.

The noise energy, N_o, in this link is calculated from $N_o = kT_s$ where $k = 1.38 \times 10^{-23}$ J/K and T_s is the system noise temperature. Assuming a receiving parametric preamplifier with an equivalent temperature of T = 75 K, and including the 2-dB (1.58) power loss in the receiver's antenna transmission line, we find

$$T_s = \left(1 - \frac{1}{1.58}\right) 290 + 75 = 182 \text{ K} \qquad (1)$$

and, consequently, $N_o = 2.51 \times 10^{-21}$ joules (-206 dBJ).

*We feel that this size of array is realistic, given the configurations of the aircraft that are likely to carry these.

Table 1

PACSAT LINK PARAMETERS

Transmitted power (20 kW for broadcasting)	(+)	43 dBW
Transmitting antenna gain (1.5-m dish at 8 GHz, η = 55%)	(+)	39.5 dB
Transmitting antenna pointing loss (antenna boresight off LOS to satellite)	(-)	1 dB
Transmitter line losses	(-)	2 dB
PACSAT radar cross section (10^6 m^2 for 1.5-km array*)	(+)	60 dB
Spreading factor $(4\pi)^3 R^4_{max}/\lambda^2$ (λ = 3.75 cm, R_{max} = 15,000 km for h = 10,000 km)	(-)	348.5 dB
Receiving-antenna line losses	(-)	2 dB
Receiving-antenna pointing error (antenna boresight off LOS to satellite)	(-)	1 dB
Phased-array receiving antenna (3-m × 3-m array, η = 55%, and we assume that the projected area of the array is $1/\sqrt{2}$ times its actual area)	(+)	45 dB
Received signal level	$\approx$	-167 dBW

*Longer arrays can be used; however, our previous investigations have used 1.5 km as a typical array length. For consistency this length is also used in this report.

For a bit error rate on the order of 10^{-3}, and using Viterbi encoding with K = 5, R = 2/3, the required energy per bit is

$$E/N_o = 4 \text{ dB} \quad . \tag{2}$$

By comparing the received power (-167 dBW) with the required energy (-202 dBJ) to achieve the 10^{-3} error rate, we can determine the

communication speed that can be supported by this link, which is (202-167) = 35 dB or B = 3162 bits/s. To enhance resistance to jamming,* we assume a frequency-hop system, and divide the required 400-bit message into two groups of 200 bits. The time required to transmit the 200-bit message is T_1 = 0.065 s. Because T_1 is greater (by a factor of ~1.4) than the uncertainty in the signal propagation time from transmitter to receiver, the transmitter is not required to provide "dead" time between successive transmissions of the message. Furthermore, multiple receivers are not required for the reception of a frequency-hopped message.

To determine the total time required to transmit the message to all stations within ±23° of the satellite axis, we note that the coverage area centered about the subsatellite point subtends a solid angle of 0.5 ster at the satellite. In turn, the solid angle occupied by the satellite's radiation pattern is given by

$$2\pi \sin \beta(d\beta) \cong \frac{2\pi(0.886)\lambda}{L} = 1.39 \times 10^{-4} \text{ ster} \qquad (3)$$

where†

$d\beta$ = Half-power beamwidth of PACSAT useful reradiation

β = Angle of returned signal relative to PACSAT axis

L = Length of array

λ = Wavelength

Hence, the number of times the message must be retransmitted, assuming that the annuli of the reradiation pattern on the ground are made to overlap at their -3 dB points, is $0.5/1.39 \times 10^{-4} = 3.6 \times 10^{3}$ (repeats), and the total message time, T, is

$$T = (3.6 \times 10^{3})(1.3 \times 10^{-1}) = 4.68 \times 10^{2} \text{ s} \qquad (4)$$

or

$$T = 7.8 \text{ min} \quad . \qquad (5)$$

---

*Jamming is discussed in Section II-B-4.

†These parameters are discussed more fully in various SRI technical reports regarding the PACSAT.

The reply message is relayed over the same link by transmitting 1000 W through the conformal array. For a 3-m-by-3-m array with elements spaced every $\lambda/2 = 0.0188$ m, the total number of elements is approximately 2.5×10^4 and the total power per element is $1000/2.5 \times 10^4 = 4 \times 10^{-2}$ W. This low value for the power per array element is within the capabilities of the structure, provided a suitable corporate waveguide feed is used. Our discussions with Mr. Bob Munsen at Ball Brothers support the feasibility of building a 1/2-to-1-inch-"thick" phased array with the appropriate waveguide feed.

The reply link differs from the broadcast link only in transmitter power; the response can be sent at a rate of

$$B_r = (3162)\,\frac{1{,}000}{20{,}000} = 158 \text{ bits/s} \quad . \tag{6}$$

This rate is regarded as adequate for transmitting a reply message.

2. Link Operating Procedure

The transmitter and all receivers direct their antennas to the array, using satellite ephemeris data and knowledge of their position and attitude.

The 100-kHz bandwidth of the array is limited by its length, which also controls the beamwidth and area of the earth footprint. Using the fact that a frequency change corresponding to the 3-dB bandwidth moves the footprint by a 3-dB beamwidth, we multiply 3.6×10^3 repeats by 1000 to obtain a total bandwidth requirement of 360 MHz, which is divided into 3600 discrete frequency bands each 100 kHz wide.* The first operational step is to order or group this set of 3600 frequencies into a sequence developed by a quasirandom process. The time to transmit all 3600

*By making this assumption we accept the fact that the received signal will be 3 dB weaker in some locations than in others. However, each part of the message is received twice in these "crossover" areas, so the total received energy per bit is the same as that received in the most favored areas. Procedures are being investigated to make use of this energy addition.

frequencies is 3.9 minutes. At the end of this time the process will be repeated, using a new quasirandom sequence. In this way, each channel will be revisited and all intended listeners will be reached once each 3.9 minutes.

The succession of quasirandom sequences, which must be duplicated at all receivers, represents the code of the day. It can be generated by shift-register techniques that are discussed in the literature on radar and communication systems.

Using the appropriate code, each receiver tunes its local oscillator to track the frequency being radiated, including corrections for estimated Doppler shift and signal delay caused by path length. All stations are assumed to know absolute time to an accuracy of 100 μs and absolute frequency to an accuracy of 10^{-7}. These values lead to tuning inaccuracies of 600 and 750 Hz, respectively, neither of which is serious in the present context. As noted in a following section, Doppler effects could cause larger frequency errors, but they can be corrected by ephemeris data and AFC or phase-lock techniques in the receiver.

The essence of the system described above is that each receiver continues to point its antenna to the satellite from which a signal might be expected and to tune its receiver to the frequency that would arrive if the transmitter were operating. When the latter condition is satisfied, the signal is received. No specific preamble is required, and the probability of missing the signal or of receiving it erroneously is low. Additional safety is provided by the fact that the whole process is repeated after 3.9 minutes.

3. Reply Procedure

Lacking knowledge of the position of the transmitter, an individual receiving station has no way of anticipating the frequency by which a message will arrive. However, it does know that the path is reciprocal and does not change extremely rapidly with time. Therefore, a reply can be sent by reusing the same frequency that brought the message. We assume the responding aircraft delivers a power of 1 kW to the

transmission line feeding the phased array. Therefore the reply rate must be reduced from the broadcasting rate by the transmit power ratio--i.e., 20 = 1 for a message rate of 158 bits/s.

To obtain the response the master station must have a receiver that tracks and follows its own radiated frequency, introducing a suitable delay to recognize the response when it comes. A considerable number of receivers following a suitable interwoven pattern must be provided if responses are anticipated from several receiving sites.

4. Jamming Resistance

The system just described is inherently very resistant to jamming. As noted, the dwell on each frequency, which is also the duration of the 200-word message, is only 0.065 s. This is also the time required for a signal to propagate 20,000 km, the shortest possible round trip to the satellite. Therefore the transmitter will have shifted to a new unpredictable frequency before any unauthorized receiving station on earth can measure and identify the frequency that was previously transmitted. The selection of frequency on a quasirandom basis, known to the transmitter and intended listeners but unknown to all opponents, precludes any effective form of track-and-follow jamming. The fact that the occupied bandwidth of 360 MHz is 1.2×10^5 times larger than the signal bandwidth of (about) 3 kHz imposes a 51-dB penalty on the jammer, who is forced to occupy the entire frequency band.

Part I of the PACSAT final report (Ref. 1) shows that a jammer with 1 MW transmitter power and a 50-ft antenna is (marginally) effective against a system with an 8-kW transmitter and a 5-ft antenna only when the jammer is within approximately 800 km of the intended transmitting annulus. This margin is not significantly affected by changing to a lower orbit and the different parameters of the airborne transmitter. Thus, even if we credit the opponent with a 10-MW transmitter and a 500-ft antenna, thereby increasing his ERP by 30 dB over the previous assumptions, the frequency agility of the new system reduces his effectiveness by 21 dB below that of the former example. Moreover, the reduced altitude of the

satellite reduces the annulus width proportionately, and the jammer can begin to be effective only if he is within approximately 15 km of the annulus that includes the intended transmitter.

Jamming against the reply will be easier because of the reduced value of transmitter power assumed. This ratio is 20:1--i.e., 13 dB. On this basis the jammer will be effective only if he is within about $15 \times 20 \approx 300$ km of the annulus from which the response originated.

5. Doppler Effects

In a 5.5-hour circular orbit, a satellite has a velocity of about 5000 m/s. The maximum corresponding Doppler effect is halved to 2500 m/s by the fact that α and β are less than 30° ($\sin 30^\circ = \frac{1}{2}$).

Doppler shift due to motion of either airborne terminal is directly proportional to the radial component of its velocity. Taking Mach 2 as the largest credible mutual speed, we have about 700 m/s for this parameter. The maximum sum of the two velocity components is 3200 m/s. The corresponding Doppler shift for either terminal is $8.0 \times 10^9 \times 3.2 \times 10^3 \div 3 \times 10^8 \approx 8.5 \times 10^4$ Hz.

We credit each terminal with knowledge of its own position and velocity and with having ephemeris data for the satellite. With this knowledge, each can make a first-order frequency correction that reduces the total error to within one bandwidth of the signal. A fast-acting AFC or phase-lock circuit is sufficient to reduce the net error to an insignificant value.

C. Straightness Requirements for PACSAT

In the previous sections, it was assumed that the PACSAT used in the communication link is perfectly straight. On this basis the maximum radar cross section RCS for the array (+60 dBsm for a 1.5-km array) was used in the calculations. In actual practice it is probable that the array will not be exactly straight. In order to account for this possibility we now consider the degradation in the array RCS as a function of random angular displacements.

In the analysis, the PACSAT is assumed to deviate from its ideal straight configuration by assuming a two-dimensional normal distribution in both position and joint angles. The resulting phase error and reduction in signal strength is then calculated.

1. Geometry

The geometry pertinent to this analysis is shown in Figure 9. The principal axis of the array is aligned with the z-axis. Each section of the array contains L elements--i.e., 100 spheres. There are a total of M sections, with M equal to either 100 or 1000 for array lengths of 150 m and 1.5 km, respectively. The incident wave lies in the x-z plane and makes an angle α with the positive z-axis. The return signal is in the direction described by a polar angle β and an azimuth angle γ.

2. Specification of the Random Angular Displacements

We begin by dividing the z-axis into M equal sections, each with a length ℓ. At each of the points so defined we select a value of x and a value of y from a normal (i.e., Gaussian) distribution. The resulting (displaced) points, which are identified as the hinge points, are now connected by a series of straight lines (wires), which are in general somewhat longer than ℓ. (A later section shows that this length deviation is unimportant.) On each straight wire there are L (100) uniformly spaced scatterers (spheres). On the average the spheres are closer to the z-axis than are the hinge points, but this fact is unimportant. The important fact, which follows from the central-limit theorem, is that the displacements of the total ensemble of scatterers is a two-dimensional Gaussian distribution with zero mean. Alternatively, polar coordinates can be used and we can say that the elements have a uniform angular distribution and a Rayleigh distribution in radial distance. The angles of the segments referred to the z-axis, and the angles between adjacent segments (wires), also obey a Rayleigh distribution.

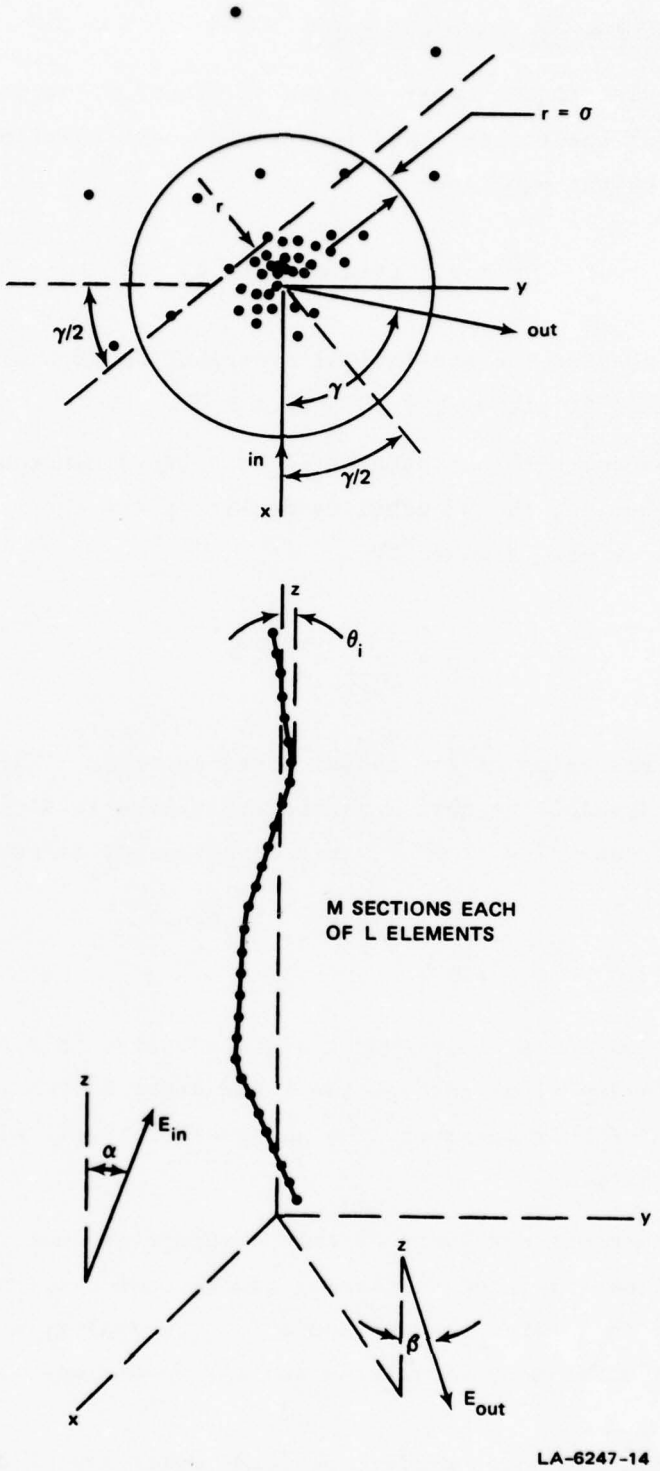

FIGURE 9 GEOMETRY OF PACSAT ARRAY

3. Evaluation of the Phase Error

Referring to the upper portion of Figure 9, we see that the phase error for each of the spheres that lies on the particular dotted line shown is given by the equation*

$$\delta = \frac{\pi r}{\lambda} \cos \frac{\gamma}{2} (\sin \alpha + \sin \beta) \text{ rad} \quad . \tag{7}$$

Our problem is to find the statistical distribution of the phase error, which becomes zero if either $\gamma = 180^\circ$ or $r = 0$.

Consistent with our assumption of a two-dimensional zero-mean Gaussian distribution, the probability density p for the radial distribution of the scatterers is given by

$$p = \frac{1}{\sqrt{2\pi}\sigma} e^{-r^2/2\sigma^2} \tag{8}$$

where σ is the rms value of the radial distance error. This function represents the probability that a particular sphere is a distance r from the z-axis. Because $r^2 = x^2 + y^2$, this equation may be rewritten

$$p = \frac{1}{\sqrt{2\pi}\sigma} e^{-x^2/2\sigma^2} \cdot e^{-y^2/2\sigma^2} \quad . \tag{9}$$

From this equation it is clear that a slice parallel to either the x- or y-axis and hence <u>any</u> slice through the total distribution is also Gaussian. By an extension of this argument, the phase error δ will also have a Gaussian distribution.

An important corollary of this argument is that the number of spheres in a slice (of fixed thickness) remote from the z-axis is smaller than the number in a slice through the axis. By analogy with the resolution of circuit noise into equal sine and cosine components, this property

*This is the relative phase difference (less multiples of 360°) between signals scattered from each sphere. For a detailed discussion on the scattering properties of the array, see Ref. 2.

has the effect of increasing the allowable distance error by a factor of $\sqrt{2}$.

4. Evaluation of Array RCS Reduction

Figure 10 gives a general idea of how the resultant signal is reduced when a large number of components of equal magnitude have a Gaussian phase distribution. Ruze (Ref. 3) and Spencer (Ref. 4) have treated a similar problem in connection with reflector antennas. Ruze's calculation lead to a 1-dB gain reduction when the rms reflector error is 0.25 rad. A 3-dB error corresponds to 0.4 rad. These numbers are applicable in our situation, because both cases treat reflection in which the electrical phase error is doubled by the "round-trip effect." A derivation of these results is included in the Appendix.

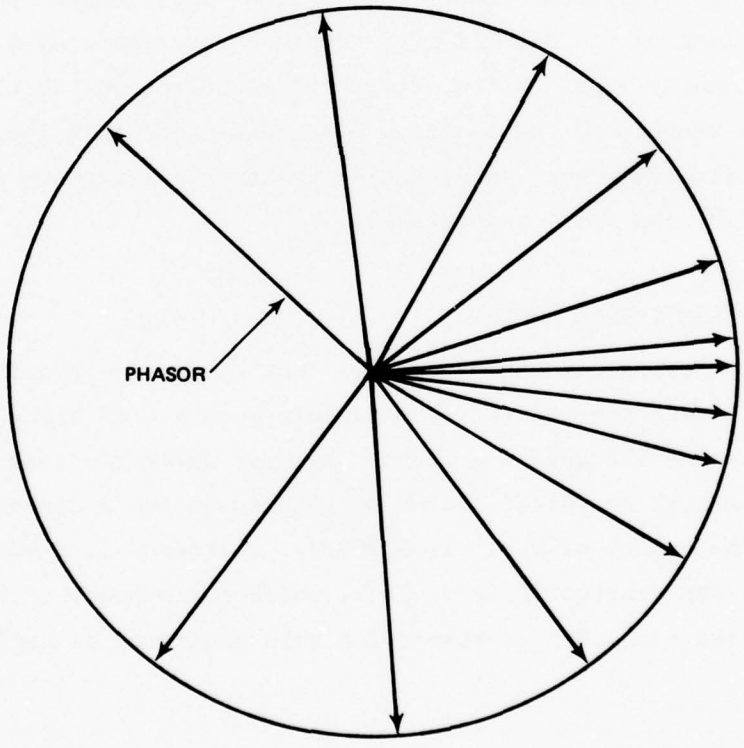

FIGURE 10 PHASOR DIAGRAM--GAUSSIAN DISTRIBUTION

A (one-way) phase error of 0.25 rad represents a displacement of $0.25/2\pi$ wavelengths. We multiply this number by the factors $\sqrt{2}$ and 10* to accommodate the independence of x and y and the fact that sin α and sin β are both approximately 0.1. (We assume $\gamma = 0$.) Combining all these terms we conclude that the rms displacement of spheres from the z-axis may be $\sigma = 0.56\lambda$ and $\sigma = 0.90\lambda$ for 1-dB and 3-dB degradations of response, respectively. At 8 GHz ($\lambda = 3.75$ cm) these displacements are 2.1 and 3.4 cm, respectively.

Again relying on analogy with the behavior of noise currents in electric circuits, we conclude that the rms displacement between two spheres chosen at random (from the end view shown in Figure 8) will be $\sqrt{2}$ times as large as the rms displacement (of each) from the origin. Therefore, we conclude that the lengths of the rms projections of the individual 100-ball segments may be 0.79λ and 1.27λ, respectively, for 1-dB and 3-dB signal reduction. The angle of each segment relative to the z-axis is given by $\theta = \tan^{-1}\sqrt{2}\,\sigma/\ell$. Because the length of a 100-element segment is nearly equal to 50λ, these values correspond to 0.91° and 1.45°, with respect to the z-axis. By extension of this logic, successive segments will have mutual angular displacements enlarged by another factor of $\sqrt{2}$, or 1.3° and 2.1°, respectively.

5. Second-Order Effect

The foregoing analysis shows that an angular displacement of 0.91° relative to the z-axis is compatible with a 1-dB signal reduction. We now reexamine the question whether angular deflections of this extent seriously perturb the distribution of spheres in the z dimension. We note that the cosine of 0.91° is 0.99987. Therefore in a 50λ (100 element) section the foreshortening is 0.0063λ, which corresponds to 0.04 rad of phase perturbation. The corresponding gain reduction is negligible.

*This factor corresponds to $\alpha = \beta \approx 6°$, which is applicable to geosynchronous altitude.

6. Summary

The analysis presented above shows that if the rms angular displacement of the array joints relative to the z-axis is $\leq 1^\circ$, then a small (≤ 1 dB) reduction in the signal-to-noise ratio (SNR) will occur in the link discussed in Section II-B. The analysis also shows that increasing the rms angular displacement to 1.5° results in a 3-dB reduction in SNR. Because these rms angular displacements are relatively small, it is necessary to consider any mechanism that may cause the ball joints to stick or freeze at angular displacements on the order of a few degrees. The only potential mechanism we have identified that could result in these displacements is the coefficient of static friction between the joint surfaces. This possibility is investigated in Section III of this report.

D. Additional PACSAT Link Considerations

The preceding sections have shown how a particular aircraft-to-aircraft communication link can be implemented via a PACSAT. It should be noted, however, that other system parameters are possible. For example, if future aircraft-to-aircraft communication systems operate at ~20 GHz, then a system comparable to the one described above can be realized by placing a 3-m-by-3-m, 20-GHz conformal phased array on all aircraft (master included). For 1 kW of available transmitter power, the 20-GHz PACSAT link (with an appropriately designed array) would support both forward and reply communication at the 3170 bits/s rate.

III COEFFICIENT OF STATIC FRICTION IN THE LIMITED-MOTION JOINTS OF THE SPACE ARRAY

A. General

The preceding section has demonstrated that the angular displacement between successive 100-element array segments must be less than 1.3° if the reduction in array RCS arising from lack of array straightness is to be limited to 1 dB or less. Because this angle is small, there is the concern that static friction in the array joints may cause them to stick or freeze at angles that would result in a decrease in the signal strength backscattered from the PACSAT. This concern is highlighted because of the fact that the loading (tension) in the joints will be very small, which might result in very high values for the coefficient of static friction μ_s between surfaces (Ref. 5).

In an attempt to avoid this potential problem, several techniques for lubricating the limited-motion joints were considered. After an extensive literature search it was decided that the best lubricant for the PACSAT is pure molybdenum disulfide because it is a space-qualified lubricant, it protects against vacuum welding of metals, and it is quite resistant to space radiation. Furthermore, MoS_2 was advertised as providing lubrication at low loads; however, no data were available for conditions corresponding to the contact forces that will exist between the working surfaces of the PACSAT joints. Consequently, an experiment was devised to measure μ_s for surfaces coated with MoS_2 and subjected to conditions that are likely to exist in the PACSAT joints where the array is deployed in a synchronous orbit. The apparatus used in the experiment and the results of the measurement of μ_s are discussed below.

B. Coefficient-of-Friction Experiment

1. Array Tension Calculations

In order to design an appropriate experiment to measure the low-pressure coefficient of friction for the working surfaces of the joint shown in Figure 5, it is necessary to calculate the tension that will exist in the array after it has been deployed and reached equilibrium (i.e., once libration and flexure have been damped). The geometry and parameters necessary for these calculations are given in Figure 11. Based on the parameters defined in this figure, the following equations* can be calculated for the equilibrium tensions T_{eq} in the array (Ref. 1):

$$T_{eq}(x) = \frac{3}{2} n^2 \sigma_1 \left[\left(\frac{L_o}{2} + \ell + L_1 \right)^2 - x^2 \right] \quad \text{(tips)} \tag{10}$$

$$T_{eq} = \frac{3}{2} n^2 \sigma_1 L_1 \left(\frac{L_o}{2} + \ell + \frac{L_1}{2} \right) \quad \text{(springs)} \tag{11}$$

$$T_{eq}(x) = \frac{3}{2} n^2 \left[\sigma_1 L_1 \left(\frac{L_o}{2} + \ell + \frac{L_1}{2} \right) + \sigma_o \left(\left(\frac{L_o}{2} \right)^2 - x^2 \right) \right] \quad \text{(main array)} \tag{12}$$

where it assumed that the springs have a negligible mass compared with other portions of the array.

For the demonstration array in a geostationary orbit, we have

n = Orbital rate = 7.3×10^{-5} rad/s

$\sigma_1 = \sigma_o$ = Linear density of array $\approx$ 0.25 kg/m

L_o = Length of main array $\approx$ 231 m

L_1 = Length of tip mass $\approx$ 15.4 m

ℓ = Length of spring $\approx$ 14.9 m

*These equations assume that the spring mass is negligible in comparison with other portions of the array. This assumption is valid for the demonstration PACSAT.

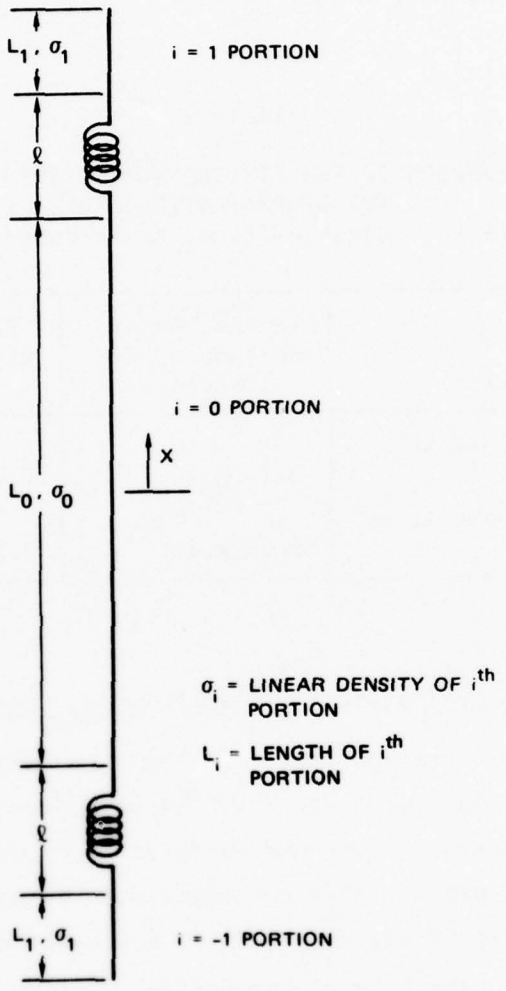

FIGURE 11 PARAMETERS USED IN TENSION CALCULATIONS

Table 2 presents the tension expected in the limited-motion joints of the array both before and after the end structures (loop and tip masses) are released. The first row of this table gives T_{eq} in the joints nearest the center of the array and the second row gives T_{eq} in the last joint at each end of the PACSAT.

Table 2

TENSION IN THE LIMITED-MOTION JOINTS
OF THE DEMONSTRATION ARRAY
(Array Length = 231 m; Brass Spheres)

Location	Tension Before Release of End Structure	Tension After Release of End Structure
Joints nearest array center	3.24×10^{-5} N	2.81×10^{-5} N
Joints nearest array end	5.08×10^{-6} N	7.26×10^{-7} N

2. Apparatus to Measure Low-Load Friction Coefficient

The most severe constraint on the experimental hardware is the requirement to measure μ_s for the limited-motion joints when the force (tension) between the working surfaces is on the order of 7.3×10^{-7} N (see Table 2). The apparatus used to make these measurements is shown in Figure 12; Figure 13 is a schematic representation of this apparatus. In this system, the contact surface between the mass (weight) and the support plate simulates the surfaces that are in contact within the limited-motion joints of the array. The micrometer head is used to set the contact force (i.e., normal force) F_N between the weight and the plate. This force is given by

$$F_N = mg \cos \theta \qquad (13)$$

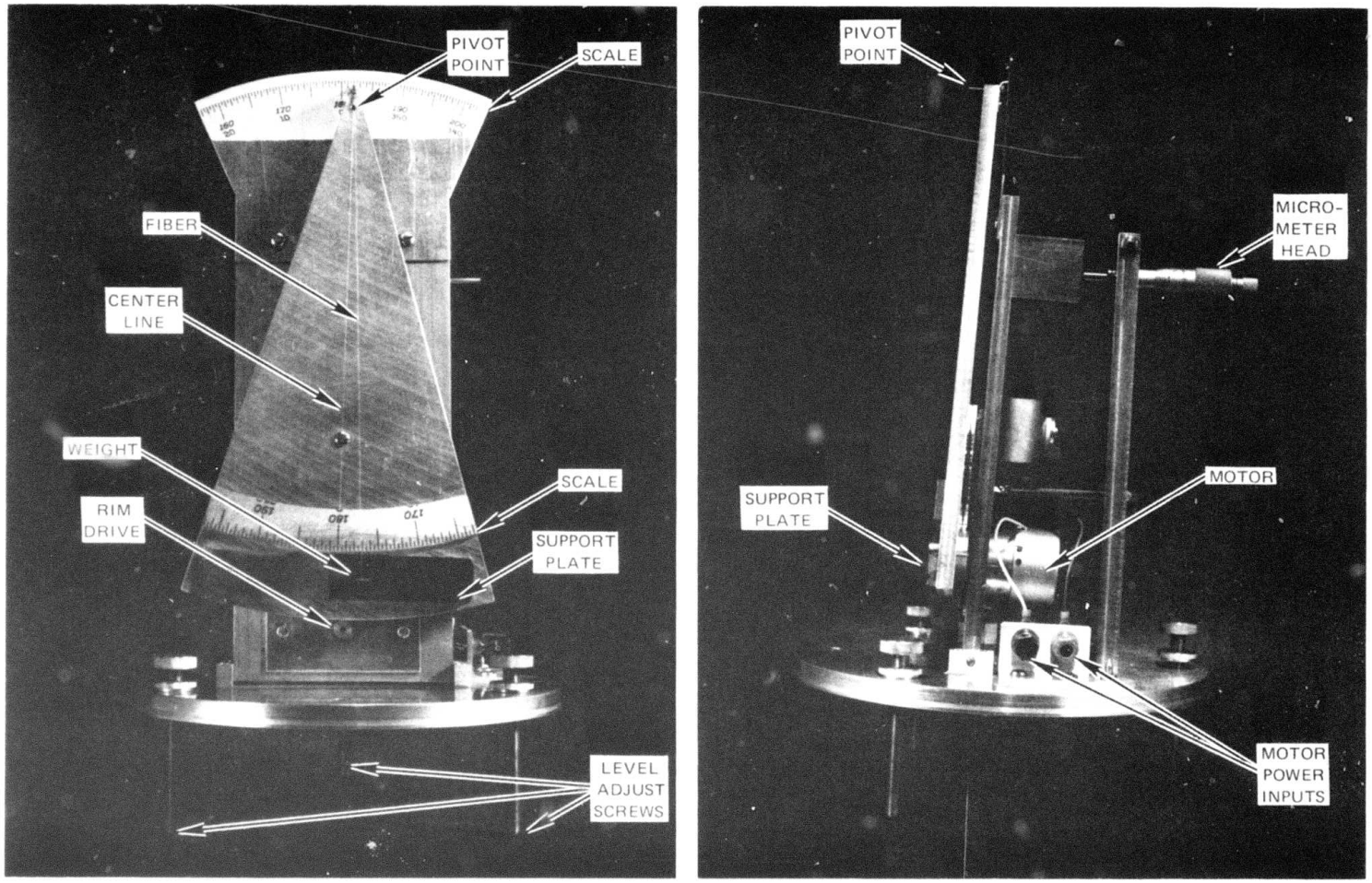

LA-6247-17

FIGURE 12 EXPERIMENTAL APPARATUS FOR MEASUREMENT OF LOW COEFFICIENT OF STATIC FRICTION

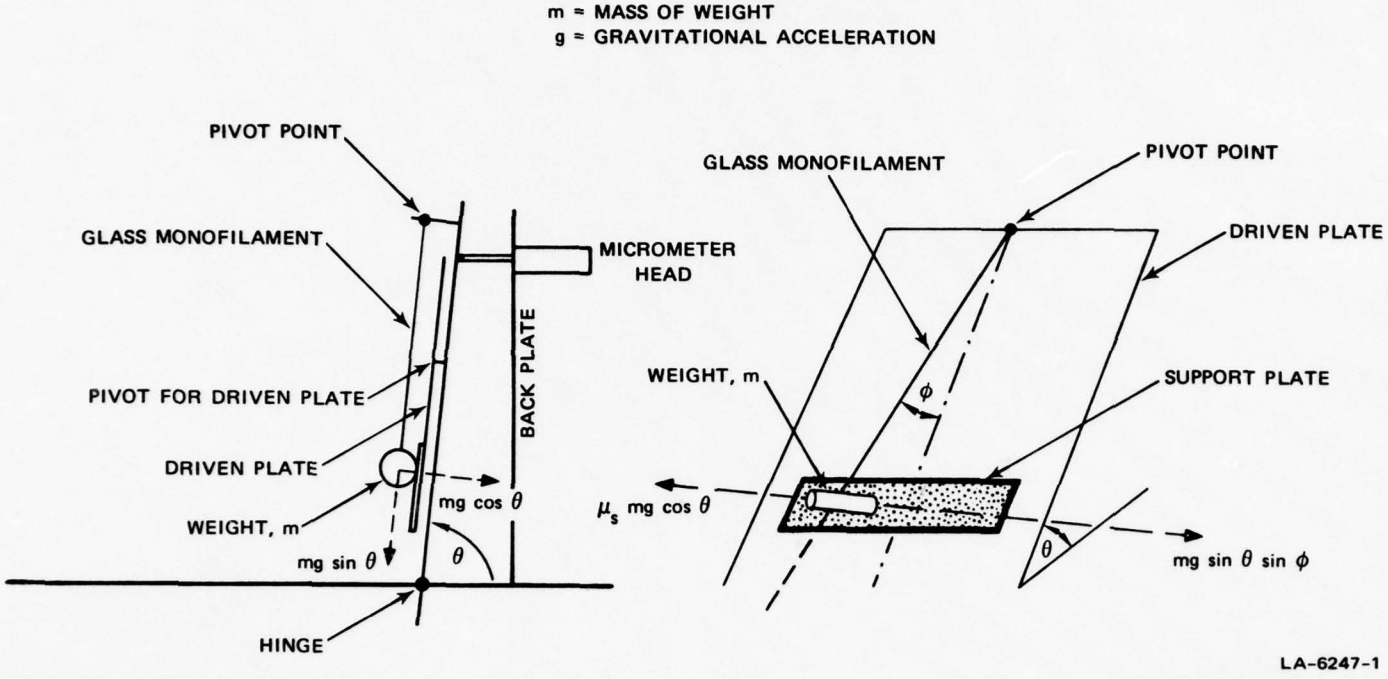

FIGURE 13 SCHEMATIC REPRESENTATION OF EXPERIMENTAL APPARATUS FOR MEASUREMENT OF LOW COEFFICIENT OF STATIC FRICTION

where

m = Mass of weight

g = Gravitational acceleration

θ = Angle between driven plate and the vertical backplate (see Figure 13).

To measure μ_s for a particular value of F_N (and hence θ), the driven plate is rotated about the pivot point by the dc motor. As the driven plate rotates, a force F_p parallel to the support surface acts on the weight and tends to cause the weight to slide. This force is given by

$$F_p = mg \sin\theta \sin\varphi \tag{14}$$

where φ is defined in Figure 13. The static friction force at a specific θ is

$$F_f = \mu_s F_N = \mu_s mg \cos\theta \quad . \tag{15}$$

To measure μ_s the driven plate is rotated until the weight begins to slide. At the instant the mass commences to move, the value of φ_1 is recorded by observing the scales on the apparatus (Figure 12). For this value of φ_1 (i.e., when $F_p = F_f$) we obtain

$$F_f = \mu_s F_N = \mu_s mg \cos\theta = mg \sin\theta \sin\varphi_1 \quad . \tag{16}$$

Hence, at the instant the weight starts to slip, μ_s can be found from

$$\mu_s = \tan\theta \sin\varphi_1 \quad . \tag{17}$$

The experiment therefore consists of setting θ to establish the desired F_N and then rotating the support plate until the weight slips. When this occurs, φ_1 is recorded and μ_s is calculated. Of course, several (at least ten) measurements of μ_s were made for each θ setting in order to obtain a statistically meaningful measure for the coefficient of static friction. Details on the design of the apparatus are as follows:

(1) To keep the weight manageable in size (for machining and handling), and to provide a contact area between working surfaces nearly equal to that in the limited-motion joints, the weight was chosen to be cylindrical in shape with a length = 0.78 cm and a diameter = 0.081 cm. The weight is made of beryllium copper BeCu and has a mass of 3.5×10^{-5} kg.

(2) The support plate was made from a machinist's parallel in order to ensure a flat, well-defined surface.

(3) To achieve a contact force of 7.2×10^{-7} N between the weight and the support surface,

$$(m)(g) \cos \theta = 7.2 \times 10^{-7} \tag{18}$$

$$\theta = 89.88^{\circ} \quad . \tag{19}$$

For a contact force of 3.3×10^{-5},

$$\theta = 84.40^{\circ} \quad . \tag{20}$$

These values for θ bound the range that must be accommodated by the micrometer in order for the contact force to cover the range listed in Table 2.

(4) To simulate the environment in which the joints must operate, the apparatus was constructed to fit inside a vacuum chamber. This chamber constrained the maximum height of the apparatus to be approximately 38 cm (15 inches). Correspondingly, the support fiber (Figure 12) for the weight was limited to a maximum length of 28 cm (11 inches).

(5) The support fiber is a monofilament glass strand whose mass is at least one order of magnitude less than that of the BeCu weight. This mass ratio was necessary to ensure that the fiber did not bias the results obtained from the experiment.

(6) The drive motor was chosen on the basis of minimizing vibrations that could invalidate the experimental results. Extensive measurements at several motor speeds and contact forces were made to verify that the motor did not cause the weight to slip prematurely.

3. Experimental Results

A series of measurements were made of φ_1 over a range of values for θ that correspond to range of force (i.e., tension) that will exist in the array from its tip to its center. The results of these measurements are presented in Figures 14 through 18. Each point plotted represents an average of at least ten measurements. Error bars indicate plus and minus

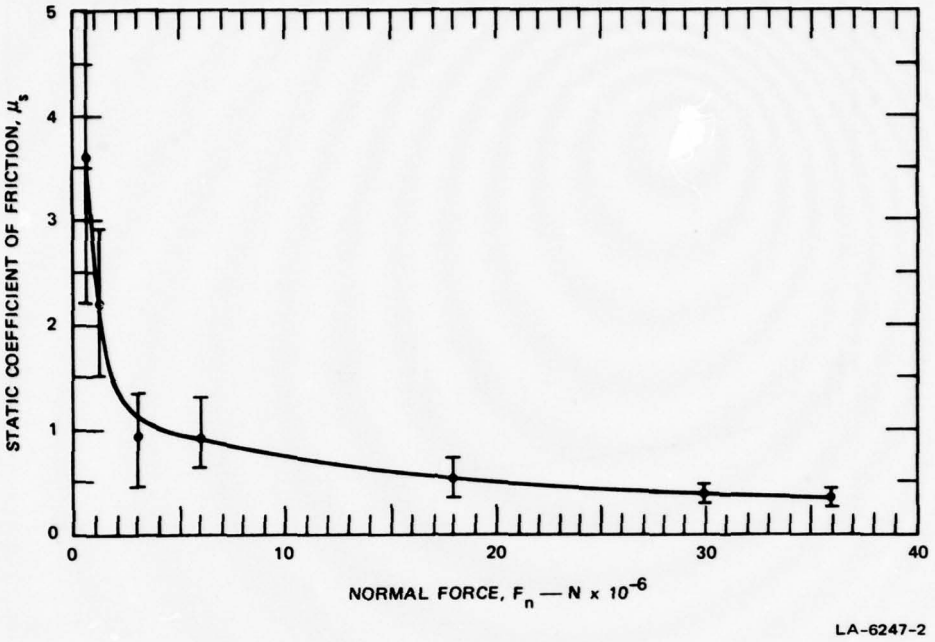

FIGURE 14 μ_s FOR UNLUBRICATED SURFACES — MEASUREMENTS MADE AT STANDARD ATMOSPHERIC PRESSURE

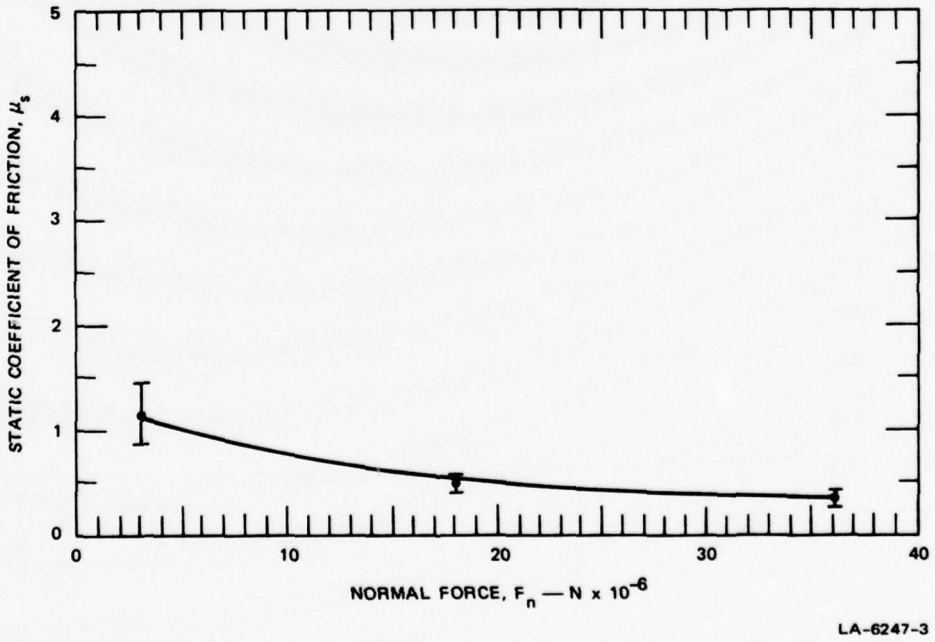

FIGURE 15 μ_s FOR UNLUBRICATED SURFACES — MEASUREMENTS MADE IN A 10^{-5} TORR VACUUM

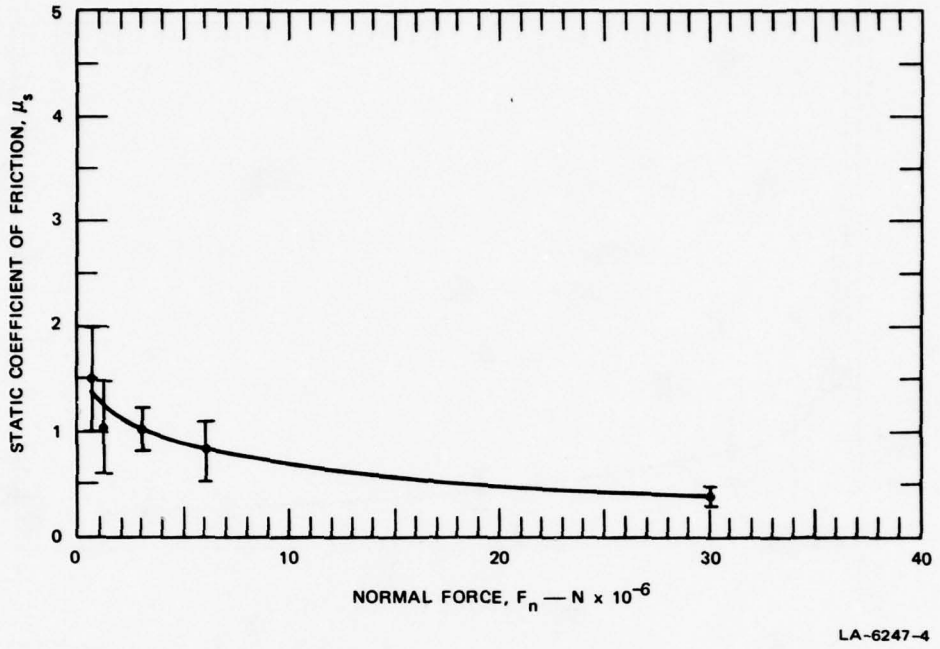

FIGURE 16 μ_s FOR SURFACES BURNISHED WITH MoS_2 — MEASUREMENTS MADE AT STANDARD ATMOSPHERIC PRESSURE

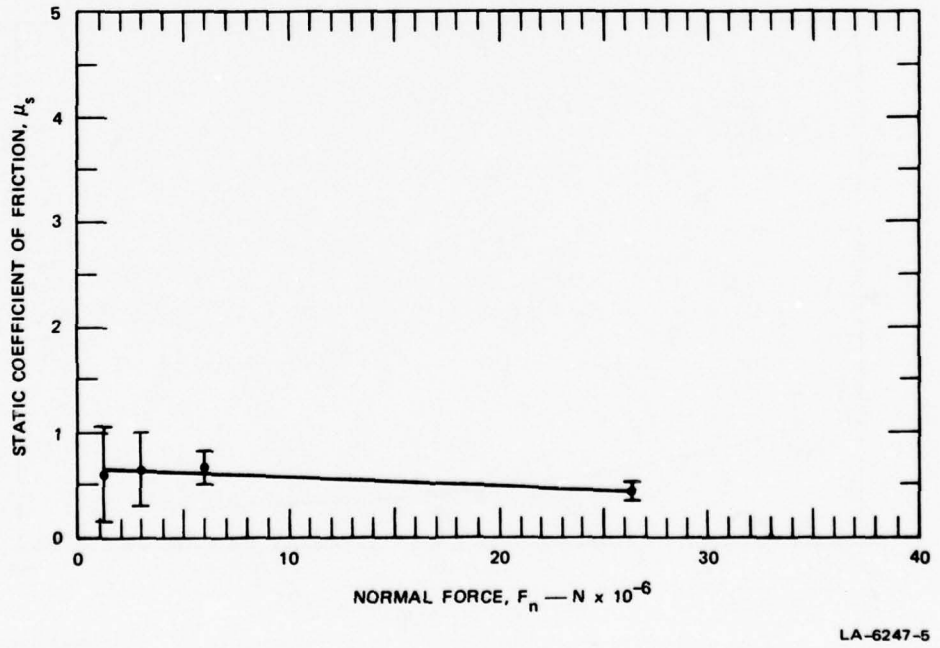

FIGURE 17 μ_s FOR SURFACES BURNISHED WITH MoS_2 — MEASUREMENTS MADE IN A 10^{-5} TORR VACUUM

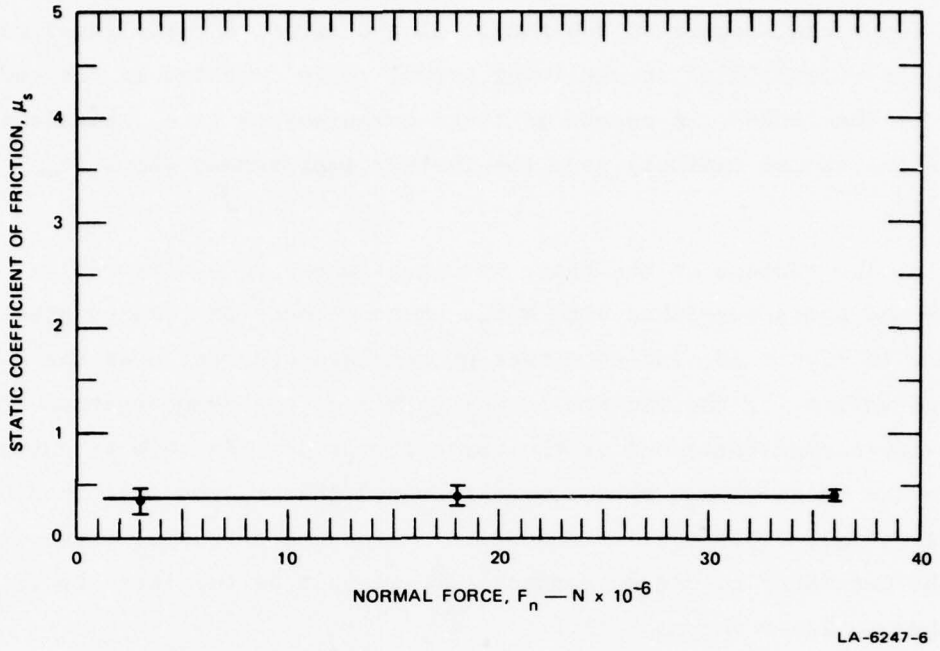

FIGURE 18 μ_s FOR POLISHED SURFACES BURNISHED WITH MoS_2 -- MEASUREMENTS MADE IN A 10^{-5} TORR VACUUM

one standard deviation of the individual measurements from the average value. Additional measurements (not shown on the graphs) were made periodically as a check on the reproducibility of the data. Good experimental reproducibility was found--namely, the average value of additional measurements fell near the center of the error bars for previous measurements.

The first series of measurements used a flat, unpolished, steel machinist's parallel for the support surface. A thin fibre of glass was used to support the beryllium copper weight. Measurements at atmospheric pressure gave the results shown in Figure 14. A coefficient of friction of 0.4 was obtained at normal forces corresponding to the center of the array. However, μ_s rises steadily as the normal force is decreased. These measurements were then repeated at reduced pressure (10^{-5} Torr) and the same behavior was found, as shown in Figure 15.

Figure 16 shows the effect (at atmospheric pressure) of burnishing both the weight and the (unpolished) support plate with powdered MoS_2. The behavior was similar to Figures 14 and 15 at the higher

normal force that occurs in the center of the array, but the magnitude of μ_s did not rise as high at the lower normal force expected in the end joints of the PACSAT. A repeat of these measurements (i.e., burnished MoS_2 in the vacuum chamber) gave the further improvement shown in Figure 17.

The surface of the plate was then lapped to a mirror-like surface and again burnished with MoS_2. Measurements at reduced pressure, as shown in Figure 18, indicate that μ_s remained constant over the entire range of values for the tension in the joints of the demonstration array. At the low-normal-force end of the curve it was not possible to establish the precise value of μ_s; rather we determined that μ_s was less than 0.5. In order to get a precise determination of the end of the μ_s curve it would be necessary to use an apparatus that would be too large to fit into the available vacuum bell.

In addition to burnishing MoS_2 on the contact surface, we also tried a spray-on coating of MoS_2 that included an inorganic, air-curing, resin binder. The results obtained for μ_s corresponding to this technique for applying the MoS_2, are not shown because the spray-on lubricant was not found to be as effective as the burnished lubricant at low loadings. This observation is in agreement with other research* that has also shown that rubbing or burnishing MoS_2 onto metal surfaces is more effective in reducing the coefficient of friction than applying the lubricant with various binders.

4. Effects of μ_s on Radar Cross Section of the Array

The experimental measurements have demonstrated that a burnished coating of molybdenum disulfide on the working surfaces of the limited-motion joints will prevent an increase in the static coefficient of friction in vacuum for the extremely light loadings that occur at joints near the ends of the PACSAT in a geostationary orbit. In particular, we have found that $\mu_s = 0.4$ over the entire range of tension expected in the demonstration array at this altitude.

*See p. 304 of Ref. 6.

Using this experimental result, we can now calculate the residual offset angle between adjacent array segments that can occur as a consequence of the static friction in the joints. The maximum offset angle θ_{max} that static friction can support occurs when

$$\tau_r = \tau_f \tag{21}$$

where

τ_r = Restoring torque in the limited-motion joints due to the tension in the array

τ_f = Frictional torque in the limited-motion joints.

The restoring torque, which tends to straighten the array, is given by

$$\tau_r = T_e \ell \sin \theta_i \tag{22}$$

where

T_e = Tension

ℓ = Length of array segment

θ_i = Angle between adjacent segments

and the frictional torque, which tends to prevent the array from straightening, is given by

$$\tau_f = T_e \mu_s r \tag{23}$$

where r is the radius of the pivot ball in the limited-motion joint. Hence, from Eq. (21), the maximum offset angle is

$$\theta_{max} = \text{arc sin} \frac{\mu_s r}{\ell} \quad . \tag{24}$$

Numerical values for μ_s, r, and ℓ are 0.4, 1.5×10^{-3}m, and 1.5 m, respectively, which result in

$$\theta_{max} = 0.023 \text{ degree} \quad . \tag{25}$$

This angle is about 50 times smaller than the value corresponding to a 1-dB degradation in the array RCS that results from lack of straightness of the array. Thus no significant decrease in the backscattered signal and from the array will occur due to friction in the limited-motion joints.

5. Damping of Flexural Motion in the Array by Friction in the Limited-Motion Joints*

In this subsection the damping in the array of flexural motion that results from the friction in the limited-motion joints is calculated. In order to make the analysis tractable, it is assumed that the array can be modeled as being comprised of stiff segments 1.5-m long connected by limited-motion ball-and-socket joints. It is also assumed that dissipative losses caused by the friction in these joints are small and therefore that the frequencies and shapes of the flexure modes in the array can be expressed as a function of the PACSAT's orbital rate and Legendre polynomials (Ref. 1), respectively. Finally, the damping springs and the end masses connected to the array are neglected in this analysis.†

Given the above assumptions, the tension T_e in the array is given by

$$T_e(x) = \frac{3}{2}\frac{M}{L} n^2 \left[\left(\frac{L}{2}\right)^2 - x^2\right] \tag{26}$$

where

M = Mass of the array

L = Length of the array

n = Orbital frequency of the array (rad/s)

x = Distance measured toward either end of the array from its center.

The work done by friction in a joint when the array changes from a straight configuration to the shape y(x) (i.e., the work done in a quarter cycle) is

$$W = \int_{-\frac{L}{2}}^{\frac{L}{2}} AT_e \frac{d\theta}{dx}\, dx \tag{27}$$

---

*The analysis given in this section is taken from an informal memorandum written by S. B. Batdorf of the Aerospace Corporation entitled "Coulomb Damping of a Chain in Orbit," dated October 1976.

†Neglecting the effect of these structures greatly simplifies the mathematics. By doing so, a lower bound on the rate of damping of the flexural modes is obtained.

$$= 2\int_{o}^{\frac{L}{2}} AT_e \frac{d^2y}{dx^2}\, dx \qquad (28)$$

where

θ = Angle of the joint relative to the local vertical

A = Constant of proportionality

and the kinetic energy, KE, associated with this flexural motion is

$$KE = \frac{M}{L}\omega^2 \int_{o}^{\frac{1}{2}} y^2\, dx \qquad (29)$$

where ω is the frequency of the flexural mode(s) associated with the shape y(x).

For the purpose of illustration, consider the damping of the second flexural mode in the plane of the orbit of the array. This mode has the form of the second Legendre polynomial,

$$y(x) = 0.5\, y_o \left[3\left(\frac{x}{a}\right)^2 - 1\right] \quad . \qquad (30)$$

In this equation, y_o is the displacement of the array tip from the local vertical due to the second flexural mode and a = L/2. Substituting this expression for y(x) into Eq. (28), we find that the work of friction for one complete flexural cycle is

$$4W = 8A\left(\frac{3y_o}{a^2}\right)\frac{3}{2}\frac{M}{L}n^2 \int_{o}^{a}\left(a^2 - x^2\right) dx$$

$$= 12A\, y_o\, M\, n^2 \quad . \qquad (31)$$

Similarly, the kinetic energy in the second mode is given by

$$KE = \frac{M}{L}\omega^2 a \int_0^1 \frac{y_o^2}{4}\left(9\xi^4 - 6\xi^2 + 1\right) d\xi$$

$$= 0.1\ M\omega^2 y_o^2 \qquad (32)$$

which equals $0.9\ Mn^2 y_o^2$ because for this mode $\omega^2 = 9n^2$.

If the friction is small and if there is negligible coupling between modes,

$$\frac{\Delta(KE)}{KE} = \frac{4W}{KE} = 13.33\ \frac{A}{y_o} \qquad (33)$$

and because the kinetic energy is proportional to y_o^2, we find that

$$\frac{\Delta y}{y_o} = \frac{1}{2}\frac{\Delta(KE)}{KE} = 6.67\ \frac{A}{y_o} \qquad (34)$$

or

$$\frac{\Delta y}{\text{cycle}} = 6.67\ A \quad . \qquad (35)$$

Thus, for friction damping the decrease in tip amplitude per cycle is a constant (i.e., the vibration amplitude decreases linearly with time).

To evaluate A, we note first that for a given tension T_e in a joint, the work done by friction is proportional to the change in angle that occurs at the joint as the array flexes. Thus, for a single joint turning through an angle θ,

$$W = T_e A\theta \qquad (36)$$

from which it follows that $T_e A$ is the frictional torque. Referring to the preceding subsection, we note that the frictional force in the bearing is given by

$$F = \mu_s T_e \qquad (37)$$

and the frictional torque τ_f is

$$\tau_f = \mu_s T_e r \tag{38}$$

where r = radius of the pivot ball in the joint. Equating τ_f to $T_e A$ we find that

$$A = \mu_s r \tag{39}$$

and therefore

$$\frac{\Delta y}{\text{cycle}} = 6.67\ \mu_s r \tag{40}$$

or, for a geostationary array,

$$\frac{\Delta y}{\text{day}} = 4\ \frac{\Delta y}{\text{cycle}} \simeq 27\ \mu_s r \quad . \tag{41}$$

This result shows that the decrease in tip displacement per day is independent of the mass and length of the array and depends only on the radius of the pivot ball and the joint's coefficient of friction.

Taking $\mu_s = 0.4$ and $r = 1.5 \times 10^{-3}$ m, we find that an initial displacement y_o of the end of the array decreases at a rate of 1.6 cm per day; hence, for $y_o = 1$ m, the flexure would be damped in about 62 days. This rate of damping is felt to be adequate for the applications identified for the array.

It should be noted that this damping rate increases for higher-order flexured modes and/or for arrays in lower orbits. This comes about because w and/or n increase (respectively) for these conditions.

Although values of dynamic friction are usually several times smaller than those for static friction, they are not used in our damping calculations because the angular velocities are so low that continuous motion is improbable. Therefore, μ_s is the appropriate coefficient for the above analysis.

IV COEFFICIENT OF DAMPING OF SPRING WIRE

A. General

Libration damping for the demonstration PACSAT is accomplished by means of extensional coil springs located near the ends of the array. The need for these springs and their design and construction is discussed in Section II-A of this report and is covered in depth in Ref. 1. This damping system is based on the lossy-spring concept developed by the Applied Physics Laboratory (APL) at Johns Hopkins University. The effectiveness of such springs for libration damping was demonstrated in the TRAAC series of gravity-gradient-stabilized satellites.

Extensional oscillations of these coiled, libration-damping springs strain the wire in torsion; hence, the damping capacity of such a spring can be measured by use of a torsional pendulum. In the early 1960s, APL utilized such a pendulum to make extensive measurements on the damping capacity of coated wires. In their experiments, torsional pendulums were constructed by using inertia hoops suspended by the wires whose damping characteristics were to be measured. The hoop was allowed to oscillate in a vacuum chamber and the damping coefficient, defined as the percent energy loss per cycle of oscillation, was determined by measuring the amplitudes of successive oscillations.

After experimenting with several wires for the springs, APL found that considerable damping of torsional energy was exhibited by beryllium copper BeCu wire plated with a thin coating of cadmium. Furthermore, it was observed that the damping coefficient for cadmium-plated wires was nearly constant for periods ranging from 2 to 55 minutes.

Because the APL satellites flew at a relatively low altitude, where the libration period is approximately 55 minutes, tests were made only for periods up to this duration. It has been speculated that the damping could decrease for oscillations with longer periods, but no adequate analysis of the damping mechanism exists to predict whether this would

occur. Hence, for a gravity-gradient-stabilized satellite in synchronous orbit, for which the libration periods are on the order of six hours, it is not possible to predict the libration damping available from such springs. To obtain the needed data, SRI decided to attempt an experiment to measure this damping at the longer periods. At the outset, it was recognized that a torsional pendulum with a six-hour period would be an extremely sensitive device and that accurate measurements would be difficult; however, no alternate technique was found to obtain the necessary data.

B. Design of Experiment

The period of oscillation, τ, of a torsional pendulum with all the mass concentrated at radius R from the torsion-wire support point, as shown in Figure 19, is given by

$$\tau = \frac{R}{r^2} \left(\frac{8\pi ML}{G} \right)^{\frac{1}{2}} \tag{42}$$

where

G = Modulus of the wire in torsion
  = 5×10^{10} N/m^2 for BeCu

L = Length of wire

r = Radius of wire

M = Mass of pendulum.

If the pendulum is completely supported by the wire, the pendulum's maximum weight W_m is related to the yield strength σ of the wire by the following equation:

$$W_m = mg = \pm r^2 \sigma \quad . \tag{43}$$

The most suitable location available for the pendulum was in our High Bay area, where the wire length is limited to about 9 m. In addition, the analysis presented in Ref. 1 shows that the optimum wire diameter for the PACSAT application is 0.0254 cm. Given that L = 9 m, r = 0.0127 cm, and $\sigma \approx 6.9 \times 10^8$ N/m^2 for BeCu, the desired six-hour period results in a minimum pendulum radius, R, of 2.7 m (9 ft). This parameter is found by substituting Eq. (43) into Eq. (42), which results in

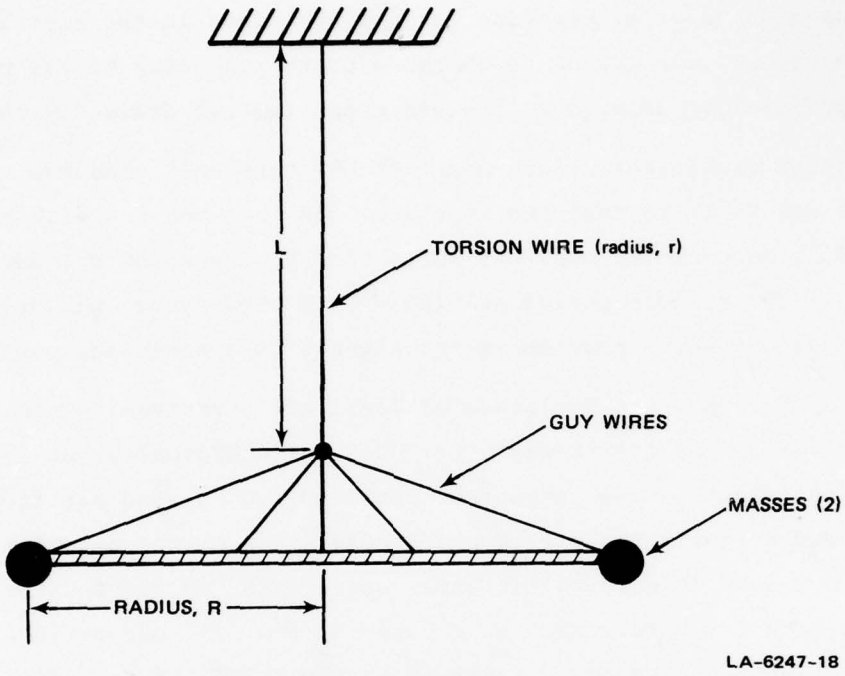

FIGURE 19 TORSIONAL PENDULUM

$$R = \frac{\tau r}{\pi}\left(\frac{Gg}{8\sigma L}\right)^{\frac{1}{2}} = 2.7 \text{ m} \quad . \tag{44}$$

Experiments at APL showed that the damping provided by air at ambient pressure exceeded the damping provided by the wires they investigated. Hence, they were forced to conduct their experiment in a vacuum. Because the minimum radius of the pendulum for our measurements is 2.7 m, an extremely large vacuum chamber would be required for our experiment. Because of the expense of renting such a large vacuum chamber,* an alternate approach was devised. The central idea of our approach was to use an enclosure surrounding the pendulum. This enclosure would be servo-driven to follow the motion of the pendulum, thereby forcing the air surrounding the pendulum to move with it. Consequently, it was expected that the air would not influence the pendulum's motion. In addition to

*A suitable chamber is available at Aeroneutronics Ford. The cost for using this chamber is on the order of $75,000.

serving as a means of eliminating air perturbations in the experiment, the enclosure would allow us to obtain a chart recording of the pendulum's angular position by using a multi-turn potentiometer driven by the enclosure.

A rather crude preliminary model of the torsional pendulum with servoed enclosure was built to test the approach. In this model a disk pendulum supported by an unplated wire was surrounded by a shallow cylindrical enclosure. The maximum period available with this system was 0.5 hour. A simple optical servo provided error signals to a servo-followup system.

During testing, the amplitude of oscillation variously grew or decayed very gradually. The growth was attributed to such problems as imperfect centering of the pendulum, imperfect servo follow-up, and air flow around the cylinder during acceleration and deceleration of the pendulum. Nonetheless, the results were sufficiently encouraging to warrant the construction of a full-scale apparatus capable of a six-hour period. A linear pendulum was suggested to simplify construction and to minimize the air-flow problem.

C. Full-Scale Experimental Apparatus

An annotated photograph of the experimental apparatus is shown in Figure 20. The 6-m plywood box surrounding the pendulum is supported at each end by a heavy-duty bicycle wheel mounted at an appropriate angle to provide minimum rolling resistance for the enclosure. A servo motor, with integral tachometer generator, drives one of the wheels through a small roller via a large-ratio gear box. A pivot, free from vertical constraint, at the center of the enclosure defines the axis of rotation. Vertical support for the enclosure and protection for the support wire from air drafts are provided by a 17.8-cm-diameter aluminum tube extending upward through a bearing fastened to the girders of our High Bay ceiling.

The test wire is supported above the middle of this tube by an arm fastened to the vertical girder. The pendulum itself consists of a pair of aluminum extrusions, which were selected for their streamlined shape (thereby providing minimum coupling to any air drafts that might occur within the enclosure). A 3-lb lead fishing weight at each end of the

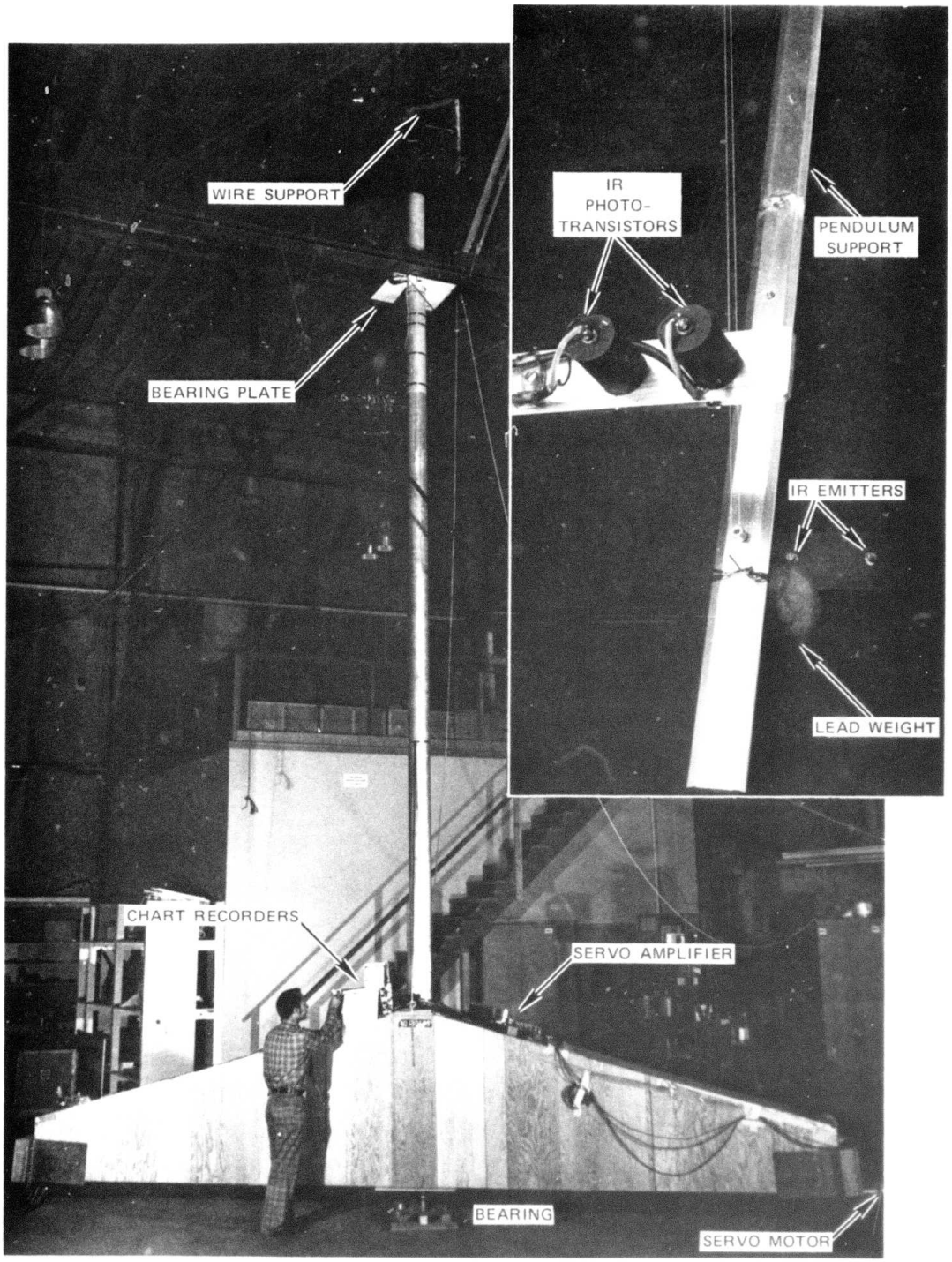

LA-6247-19

FIGURE 20 TORSIONAL PENDULUM SYSTEM TO MEASURE DAMPING CHARACTERISTICS OF WIRES

pendulum is supported by a guy wire of 0.0457-cm stainless steel model aircraft control cable. The two guy wires are joined at the lower end of the test wire at a point 0.75 m above the main pendulum member, as shown in Figure 20.

The pendulum position sensor for the servo system is mounted in the plywood box near one end of the pendulum. Two vertical infrared beams are positioned in such a manner that they pass on opposite sides of the pendulum when it is centered within the box. These infrared beams are focused on matched infrared receivers, whose outputs are fed to a differential operational amplifier. When the pendulum is exactly centered in the box, approximately one-half of the light that would otherwise reach each receiver is blocked by the pendulum. Because of the high gain achieved with the infrared electronics and the operational amplifier, offset errors as small as 0.02 cm between the pendulum's position and the center of the box can be readily detected.

Power supplies, chart recorders, and the servo electronics were all mounted on the enclosure so that only ac power needed to be supplied to the moving system. Power was provided by an extension cord suspended from the roof and wrapped around the central aluminum tube.

A ten-turn potentiometer mounted at the central pivot of the enclosure provided readout of angular position. In addition to chart records of enclosure position versus time, records of motor speed, position error, and other servo parameters were made at various times during the experiments. several servomechanism feedback loops were tried; the better of these provided tracking between the pendulum and the enclosure to within a few thousandths of a centimeter.

Calculation of the period of the experimental pendulum must include the moment of inertia of both the support member and the end weights. For the support member with mass W_1/g evenly distributed along its length, the moment is $W_1R^2/3g$, while for the end masses W_2/g it is W_2R^2/g. The period is then

$$\tau = \frac{R}{r^2}\frac{8\pi L}{Gg}\left(\frac{W_1}{3} + W_2\right)^{\frac{1}{2}} \quad . \tag{45}$$

For this pendulum, W_1 = 22.24 N, W_2 = 26.69 N, L = 7.9 m, r = 0.0127 cm, and R = 2.8 m; the calculated period is 5.7 hours.

D. Test Results

Tests were run with both plated and unplated wire samples. Examples of records of pendulum angular position versus time for both wires are reproduced in Figure 21.

The periods of oscillation for the plated and unplated wires are 5.5 and 5.8 hours, respectively. Considering the accuracy with which the parameters of the wire are known, these values are remarkably close to the calculated 5.7 hours. The period could be extended to six hours by an available adjustment of R and W.

Figure 21 shows that for the unplated wire the amplitude of oscillation grows steadily with each cycle, while for the plated wire it decays. However, widely variable growth and/or decay rates were observed for both wire samples. In addition, step changes of acceleration occasionally occurred during the experiments.

The engineers who worked with the pendulum are convinced that the behavior of the plated wire was quite different from that of the unplated one. The variance in the data was too great to support any quantitative result. A number of possible perturbing influences have been considered. None adequately explains a continuous growth in amplitude, but a few do account for the pendulum's erratic behavior.

1. Gravitational Effects

The sensitivity of the pendulum to perturbations that are generally considered negligible in typical "laboratory" experiments is exemplified by the effects resulting from the gravitational attraction between the end masses of the pendulum and masses that move with respect to the pendulum. These perturbations can be assessed in the following manner.

The torque τ_1 on the pendulum resulting from the twisting of the cadmium-plated wire is given by the following expression

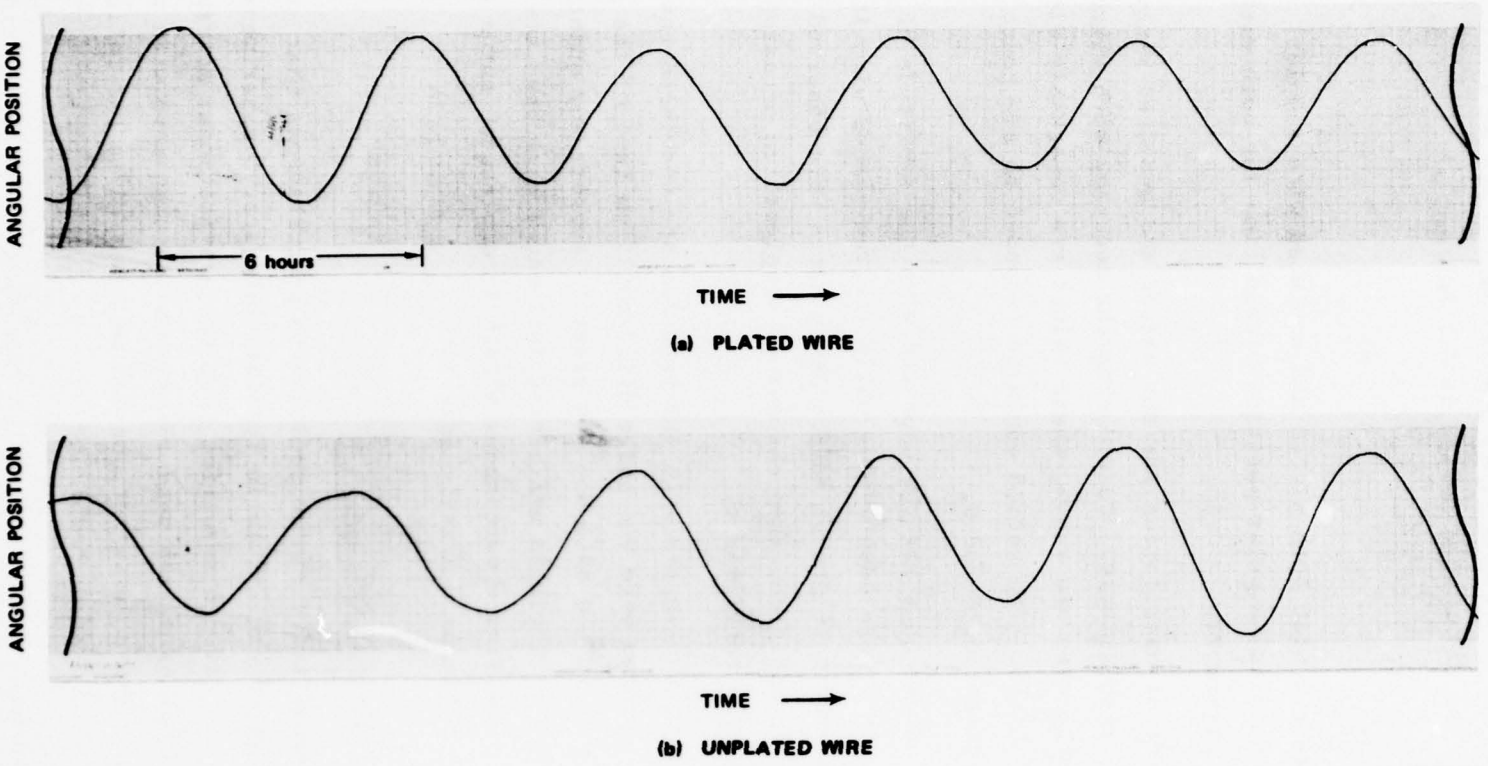

FIGURE 21 PENDULUM ANGULAR POSITION vs TIME

$$\tau_1 = \frac{JG\theta}{L} = 2.27 \times 10^{-6}\theta \quad \text{N-m} \tag{46}$$

where

θ = Angular rotation of pendulum from its neutral position ($\theta = 0$)

J = Polar moment of inertia of the support wire (4.1×10^{-16} m^4)

G = Shear modules of the support wire (5×10^{10} N/m^2)

L = Length of the support wire (9 m).

The gravitational force resulting from the attraction of one end of the pendulum to a nearby mass M is given by

$$F = \frac{MmG'}{R^2} \tag{47}$$

where

G' = Universal gravitational constant (6.67×10^{-11} N - m^2 kg^{-2})

M = Mass of object

m = Mass at end of pendulum (1.36 kg)

R = Distance between the end of the pendulum and the mass M.

In this equation we have assumed that the perturbing mass is much closer to one end of the pendulum than the other. This assumption leads to a worst-case estimate of the torques generated by these masses in the experiment. The maximum torque resulting from the force given by Eq. (47) is

$$\tau_2 = \frac{\ell}{2} F \approx 2.72 \times 10^{-10} \frac{M}{R^2} \text{ N-m} \tag{48}$$

where ℓ is the length of the pendulum (6 m). For a mass on the order of 1300 kg, τ_2 is 3.54×10^{-7} R^{-2} N-m. If we assume that this mass comes within 3 m of the pendulum, then $\tau_2 = 3.93 \times 10^{-8}$ N-m, which, when equated to τ_1 in Eq. (46) gives

$$\theta = 1.7 \times 10^{-2} \text{ rad} \approx 1^\circ \quad . \tag{49}$$

Extrapolating this result, we see that if a man ($\approx$82 kg) approaches the pendulum to within 0.75 m (2.5 ft), then he creates a torque in the system comparable to that generated by the support wire when $\theta \approx 1^\circ$.

These analytical results on the torques (and hence perturbations) caused by masses moving near the pendulum were verified empirically by placing an 80-kg mass 1 m from one end of the pendulum. The pendulum, which was stopped at its neutral position (zero angular displacement), was observed to rotate 0.07 m toward the mass. This displacement amounts to an angular rotation of about 1.3°, which is consistent with the calculations given above. Through experimentation, it was also observed that the end of the pendulum followed the mass as it was moved to either side of the pendulum's neutral position.

Although these masses can affect the dynamics of the torsional pendulum, they do not account for the increase with time of the angular displacement of the pendulum. In order to do so, masses must be made to introduce a time-variable torque with periods that are harmonically related to the period of the pendulum.* This could occur if the mass were moved in synchronism with the pendulum's 5.5-hour rotational period. The possibility of the sun, moon, and/or tides causing this type of excitation were investigated; in all cases the torques created by these objects were calculated to be at least three orders of magnitude too small to cause significant perturbations.

Gravitational perturbations do not indicate the mechanism by which the pendulum is excited; however, they do show the sensitivity of the experiment to perturbations introduced by factors that were not controlled within our High Bay area. The analysis shows that an extremely well controlled environment must be maintained if a linear torsional pendulum is to be used to measure the damping characteristics of the cadmium-plated, beryllium copper wire.

2. Electromagnetic Coupling

The pendulum and its guy wires form a loop that could couple with large electromagnetic fields to produce a torque. A rough calculation of the torque resulting from 100 amperes flowing in a single conductor a

*A torque with one-half the period of the pendulum could parametrically excite the pendulum.

few feet from the pendulum showed this to be a significant effect. Although currents of a few hundred amperes are carried in a conduit about 4.5 m from the pendulum, the return is in the same conduit and the external field is relatively small. Hence, because of the balanced lines used in the High Bay area, electromagnetic coupling should not have affected the pendulum motion.

3. Pendulum Centering

The enclosure is servoed to follow the pendulum by monitoring the position of one of its ends. Consequently, any error in centering the enclosure under the support wire results in a relative error between the position of the unmonitored end of the pendulum and the enclosure. (This error varies as the sine of the rotational angle.) Air moving past the pendulum as a result of this error could add energy and increase the amplitude of the pendulum's rotation. In order to minimize this error, a scale was located at the unmonitored end of the pendulum and the enclosure's pivot was adjusted to minimize position change with rotation. After adjustment, this error was less than ±0.1 cm, which should be sufficiently small to not affect the experiment. Nonetheless, this is the most plausible driving function we have identified.

4. Building Instability

We were initially concerned about possible motion between the High Bay roof girders and the floor. Any such motion, which would affect the pendulum's motion, is readily observed on the scale discussed in the previous paragraph. No significant motion was observed.

5. Imperfect Tracking of Enclosure

The servo system holds the controlled end of the pendulum nearly fixed (to within ±0.01 cm) relative to the box. The effect resulting from this position error is considered negligible when compared to that resulting from the error in the pendulum's centering.

E. Recommendations

Based on the experience gained during this program, the following measures are recommended for future experiments to determine the characteristics of the PACSAT libration-damping springs:

(1) The experiment should be conducted in a vacuum chamber in order to eliminate the possibility of air coupling.

(2) A symmetrical hoop inertia member should be used to eliminate any gravitational effects. This pendulum configuration is impractical for use in our High Bay area but could be implemented in the vacuum chamber.

(3) Nonmetallic construction should be employed to eliminate any possible electromagnetic coupling effects.

V CONCLUSION

Experiments were conducted to evaluate the coefficient of friction, μ_s, in the PACSAT limited-motion joints and the resulting libration damping characteristics of the springs attached to the ends of the array. The experiments to determine μ_s show that the coefficient of static friction between the lightly loaded unlubricated surfaces of the limited-motion joints can become very large (e.g., greater than 3.5). They also show that μ_s is a function of the load (tension) in the joint--μ_s being greatest for the joints near the ends of the array where the gravity-gradient tension is least. Measurements for μ_s between surfaces burnished with pure molybdenum disulfide (a solid-film lubricant) show that the coefficient can be made independent of tension in the joints. Measurements made in a vacuum for the lubricated surfaces gave $\mu_s = 0.4$. This value for the coefficient of friction in the PACSAT joints would result in no measurable degradation ($\lesssim 0.1$ dB) in the array's radar cross section as a consequence of friction in the joints; and in a geostationary array this friction gives rise to a damping of tip displacement, due to flexure, of about 2 cm per day. This damping of the primary flexural mode of oscillation for the array is adequate for future PACSAT applications.

The experiments to measure the libration-damping characteristics of the springs to be attached to the ends of the array did not provide conclusive results. This situation arose because a very large torsional pendulum was required to measure the damping coefficient of these springs when subjected to torsional strains with 6-hour periods (as they would be for a PACSAT in a synchronous orbit). The size of this pendulum resulted in its being very sensitive to spurious perturbations caused by mutual gravitational effects, motion of the ceiling from which it was hung, and air coupling. Although no quantitative data were obtained from this experiment, it was observed that springs made from cadmium-plated beryllium copper wire tend to damp torsional flexures with 6-hour periods more than do springs made of unplated wire.

More definitive torsional pendulum experiments similar to those reported here could be performed in a vacuum chamber, but would require a large and costly facility.

Appendix

EVALUATION OF LOSS VERSUS GAUSSIAN PHASE ERROR

Appendix

EVALUATION OF LOSS VERSUS GAUSSIAN PHASE ERROR

If we use δ_o to designate the rms phase error (in radians) we may evaluate the average of N phasors by writing

$$G = \frac{1}{N} \sum_{1}^{N} \cos \delta_n \tag{A-1}$$

where δ_n is governed by the probability distribution

$$p(\delta) = \frac{1}{\sqrt{2\pi}\,\delta_o} e^{-\frac{1}{2}\frac{\delta^2}{\delta_o^2}} . \tag{A-2}$$

We are interested in the limiting case in which N is very large; accordingly we substitute integrals for the coefficient 1/N and the summation in Eq. (A-1) to obtain

$$G = \frac{\int_o^\infty \cos \delta e^{-\frac{1}{2}\frac{\delta^2}{\delta_o^2}} d\delta}{\int_o^\infty e^{-\frac{1}{2}\frac{\delta^2}{\delta_o^2}} d\delta} . \tag{A-3}$$

To evaluate these expressions we use formulas 492 and 508 from B. O. Pierce (Ref. 7):

$$\int_0^\infty e^{-a^2x^2}\,dx = \frac{1}{2a}\sqrt{\pi} \qquad \text{(A-4)}$$

and

$$\int_0^\infty e^{-a^2x^2}\cos bx\,dx = \frac{\sqrt{\pi}\, e^{-\frac{b^2}{4a^2}}}{2a} \quad . \qquad \text{(A-5)}$$

Substituting $b = 1$ and $a^2 = 1/2\delta_o^2$ we have

$$G = e^{-\delta_o^2/2}$$

or

$$\ln G = -\frac{\delta_o^2}{2} \quad .$$

Thus, 1-rad rms phase error results in a 1/2-Np (i.e., 4.34-dB) loss. An rms phase error of 1/2 rad provides 1.08 dB loss.* Not surprisingly, a Gaussian phase distribution transforms into a Gaussian gain reduction.

*These phase errors are for "one-way" paths.

REFERENCES

1. W. A. Edson et al., "Passive Space Communication Array (PACSAT)," Final Report, Parts I-III, Contract DCA100-76-C-0056, SRI Project 5371, Stanford Research Institute, Menlo Park, Calif. (October 1976).

2. M. S. Frankel, "The Fabrication and Test of a Long Array Segment," Special Technical Report 4, Contract DCA100-74-C-0035, SRI Project 3323, Stanford Research Institute, Menlo Park, Calif. (October 1975).

3. J. Ruze, "The Effect of Aperture Errors on the Antenna Radiation Pattern," Nuovo Cimento, Supplement to Vol. IX, Series IX (1952).

4. R. C. Spencer, "A Least Square Analysis of the Effect of Phase Errors on Antenna Gain," Report No. E5025, Air Force Cambridge Research Center (January 1949).

5. N. Garlén, "Friction Between Single Fibres," Proceedings of the Royal Society of London, Series A, Vol. 212, p. 491 (1952).

6. E. R. Parker, ed., Materials for Missiles and Spacecraft, p. 304 (McGraw-Hill Book Company, New York, N.Y., 1963).

7. B. O. Pierce, A Short Table of Integrals (Ginn and Company, New York, N.Y., 1910).